# Climatic Impact of Amazon Deforestation—A Mechanistic Model Study

NING ZENG, ROBERT E. DICKINSON, AND XUBIN ZENG

*Institute of Atmospheric Physics, The University of Arizona, Tucson, Arizona*

(Manuscript received 22 May 1995, in final form 11 October 1995)

ABSTRACT

Recent general circulation model (GCM) experiments suggest a drastic change in the regional climate, especially the hydrological cycle, after hypothesized Amazon basinwide deforestation. To facilitate the theoretical understanding of such a change, we develop an intermediate-level model for tropical climatology, including atmosphere–land–ocean interaction. The model consists of linearized steady-state primitive equations with simplified thermodynamics. A simple hydrological cycle is also included. Special attention has been paid to land–surface processes. In comparison with previous simple modeling work on tropical climatology or anomalies, the present model is more sophisticated in predicting, with little input, most of the important meteorological variables; nevertheless, it is computationally simple. It generally better simulates tropical climatology and the ENSO anomaly than do many of the previous simple models.

The climatic impact of Amazon deforestation is studied in the context of this model. Model results show a much weakened Atlantic Walker–Hadley circulation as a result of the existence of a strong positive feedback loop in the atmospheric circulation system and the hydrological cycle. The regional climate is highly sensitive to albedo change and sensitive to evapotranspiration change. The pure dynamical effect of surface roughness length on convergence is small, but the surface flow anomaly displays intriguing features. Analysis of the thermodynamic equation reveals that the balance between convective heating, adiabatic cooling, and radiation largely determines the deforestation response. Studies of the consequences of hypothetical continuous deforestation suggest that the replacement of forest by desert may be able to sustain a dry climate. Scaling analysis motivated by our modeling efforts also helps to interpret the common results of many GCM simulations.

When a simple mixed-layer ocean model is coupled with the atmospheric model, the results suggest a 1°C decrease in SST gradient across the equatorial Atlantic Ocean in response to Amazon deforestation. The magnitude depends on the coupling strength.

## 1. Introduction

Recent general circulation model (GCM) experiments suggest a drastic change in the regional climate, especially the hydrological cycle, after hypothesized Amazon basinwide deforestation [see Dickinson (1992) for an earlier review, and references in Table 1 for more recent experiments]. These studies assume a scenario in which Amazon basinwide forests are transformed into grassland. Aside from numerous substantial changes in the atmosphere and on the ground, the most remarkable result from the majority of the models is a large reduction in evapotranspiration accompanied by a comparable or larger reduction in precipitation (typically a 20%–30% decrease), implying a decrease in moisture convergence ($\approx P - E$ in the climatological sense) in the atmosphere and a decrease in runoff on the ground. In a traditional view of atmospheric control (cf., Zeng 1994) it would be conjectured that, as evapotranspiration is reduced, the large-scale atmospheric circulation adjusts so that the moisture convergence increases to compensate (at least partially) for the loss of moisture. What a majority of these GCM experiments show is just the opposite (Table 1, some simulations do give conflicting results), that is, large-scale motion acts to further reduce moisture convergence. For example, in the work of Henderson-Sellers et al. (1993), precipitation decrease is more than twice that of evapotranspiration.

The above result has been very striking and poorly understood. Although many researchers have attempted to interpret the results in the context of individual simulation and have indicated possible mechanisms (e.g., Nobre et al. 1991; Henderson-Sellers et al. 1993), the causes and mechanisms responsible for large effects on atmospheric transport remain obscure. The question of the climatic consequences of Amazon deforestation pushes at the limit of our understanding of many processes in the tropical climate system. This work attempts to shed some light on the mechanisms and properties of the land surface that are most responsible for the simulated change, providing a unified view of the problem.

Three features related to the land surface have been identified as important to deforestation study based on theoretical grounds and GCM results. Figure 14.3 of

*Corresponding author address:* Dr. Ning Zeng, Department of Atmospheric Sciences, UCLA, Los Angeles, CA 90095-1565.

TABLE 1. Comparison of GCM simulations of Amazon deforestation. Modified from Nobre (1994, personal communication). Moisture convergence difference $\Delta C$ is calculated as the difference of $\Delta P$ and $\Delta E$ ($\Delta C = \Delta P - \Delta E$).

| | GCM Simulation of Amazonia Deforestation | | | |
|---|---|---|---|---|
| Reference[a] | $\Delta$T (°C) | $\Delta P$ (mm day$^{-1}$) | $\Delta E$ (mm day$^{-1}$) | $\Delta C$ (mm day$^{-1}$) |
| H.-S. & G (1984) | 0 | −0.6 | −0.45 | −0.15 |
| DHS (1988) | +3 | 0 | −0.56 | +0.56 |
| Lean and Warrilow (1989) | +2.4 | −1.34 | −0.85 | −0.49 |
| Nobre et al. (1991) | +2 | −1.75 | −1.37 | −0.38 |
| Dirmeyer (1992) | +1.3 | +0.09 | −0.4 | +0.49 |
| Dickinson and Kennedy (1992) | +0.6 | −1.4 | −0.7 | −0.7 |
| H.-S. et al. (1993) | +0.6 | −1.61 | −0.64 | −0.97 |
| Lean and Rowntree (1993) | +2.1 | −0.81 | −0.55 | −0.26 |
| Polcher and Laval (1993) | −0.11 | −0.51 | −0.35 | −0.16 |
| Sud et al. (1996) | +2.0 | −1.48 | −1.22 | −0.26 |
| Lean et al. (1996) | +2.3 | −0.43 | −0.81 | +0.38 |
| McGuffie et al. (1995) | +0.3 | −1.2 | −0.63 | −0.56 |
| Hahmann and Dickinson (1995) | +0.8 | −0.75 | −0.41 | −0.37 |

[a] H.-S. & G: Henderson-Sellers and Gornitz; DHS: Dickinson and Henderson-Sellers.

Sellers (1992) is an "exhaustive" plot of possible feedbacks due to change in these three factors: albedo, evaporation (soil moisture in the plot), and surface roughness length. Although the large number of possibilities appears to be overwhelming, the most important loops are few for Amazon deforestation.

Charney's (1975) albedo mechanism is frequently invoked to explain such feedback. The mechanism is that an albedo increase reduces the energy received in the whole air column above and the air cools. Then the air has to sink, with subsequent warming to compensate for the cooling, thereby inducing a downward motion superimposed on the original circulation and reducing the precipitation.

On the other hand, a large reduction in evapotranspiration alone can reduce rainfall. It does so by directly reducing the availability of moisture supply to the planetary boundary layer, therefore reducing the moist convective instability. For the Amazon, because of the unique topography, the moisture input from the Atlantic Ocean is largely precipitated out before or when it reaches the western Amazon. The basinwide evapotranspiration is expected to be mostly recycled, and it accounts for about 50% of the total precipitation (Salati 1987); however, Brubaker et al. (1993) and Eltahir and Bras (1994) have estimated it to be 30% and 25%, respectively, the rest presumably leaking out toward the south and north.

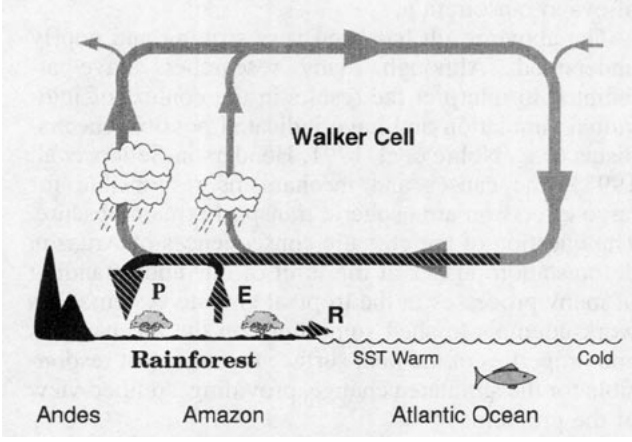


FIG. 1. Illustration of Amazon–Atlantic atmospheric circulation. Shown is a cross section along the equator. $P$ is precipitation; $E$ is evapotranspiration; $R$ is runoff.

The third factor of possible importance is surface roughness length. A smaller roughness length (as in the case of deforestation) reduces turbulent transfer of latent heat from surface to atmosphere and subsequently causes higher surface temperature and enhances outgoing longwave radiation (Dickinson and Henderson-Sellers 1988, hereafter DHS; Lean and Warrilow 1989). Surface temperature is influenced more this way than through the direct effect of albedo change (Dickinson and Kennedy 1992). However, this process is subtle and complicated by other factors such as cloud processes. Besides the role in perturbing surface energy balance, roughness length also has obvious aerodynamic effects since a smaller roughness length reduces the friction acting on the boundary-layer atmosphere (Sud et al. 1988).

While decreases in evaporation and precipitation appear to be robust in many GCM simulations, the process(es) responsible have not been found to be the same by different modelers. For instance, Dirmeyer (1992) found that albedo change is the sole important factor and that pure decrease in evaporation does not reduce precipitation. In contrast, Sud et al. (1995) found that surface roughness is the determining factor. While earnest efforts have been made by researchers

to interpret their results, the complexity of a GCM makes this hard to do. It is even harder to understand why different simulations give drastically different answers in the depiction of critical land-surface features.

Here we propose a mechanism in which a positive feedback loop exists in the climate system in the South America–Atlantic region. Figure 1 illustrates how this mechanism might work. Depicted in the figure is a west–east cross section extending from the Andes Mountains to the eastern Atlantic. The zonally asymmetric atmospheric circulation is the Walker circulation.[1] The relatively steady Walker–Hadley circulation brings in moisture at its lower branch (the trade wind) from the Atlantic, which is then precipitated over the Amazon. The latent heat released by condensation of water vapor over the Amazon, in turn, is the major driving force for the Walker circulation (Cornejo-Garrido and Stone 1977), with the land–sea contrast being the ultimate cause. The trade wind pushes the surface sea water to move westward and pile up in the west Atlantic, corresponding to a sea surface temperature (SST) gradient due to the upwelling of cold deep water in the east and the downwelling of warm surface water in the west that again feeds positively back into the Walker circulation. The zonal asymmetry is the result of the existence of this positive feedback loop in which convective latent heat release plays a central role. Thus, a perturbation to a part of this loop can be expected to cause a "chain reaction." For instance, as the forest is replaced by grass, evapotranspiration would be lower (see Table 1 for GCM results), due to the lower soil moisture content and lower efficiency of water transport in and above the canopy, etc. As a result, the precipitation and latent heat release would be less. Albedo feedback acts in the same direction to cool the atmosphere above (we ignore likely cloud feedback and diurnal cycle; see further discussion in section 6). On the other hand, higher surface temperature due to lower evapotranspiration has the opposite effect of lowering surface pressure and increasing convective instability. This latter effect would compete against the first two (e.g., Eltahir and Bras 1993) but is not expected to reverse the trend as it is the consequence. Nevertheless, this effect deserves more study. Thus, the Walker circulation would be weakened. This decreases the trade wind and SST gradient and could possibly further weaken the Walker circulation (Fig. 2). A weakening in the Walker circulation has been suggested by GCM experiments (Fig. 12d of Nobre et al. 1991; Fig. 21 of Henderson-Sellers et al. 1993). The atmospheric response to the Amazon deforestation is not unlike a warm episode of ENSO (El Niño/Southern Oscillation), in which SST anomaly causes the weakening of the Pacific Walker circulation and influences the convective regimes.

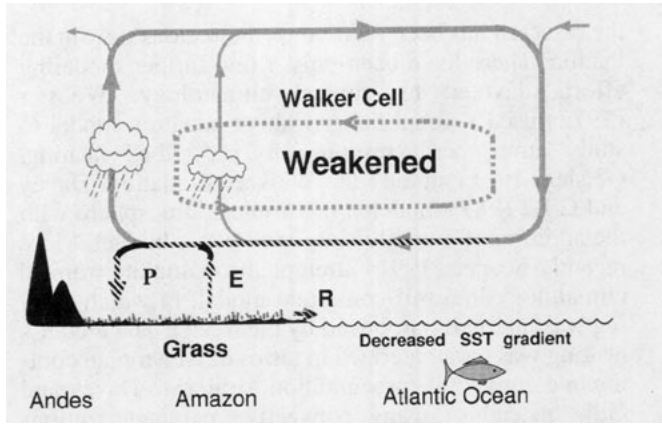


FIG. 2. Consequences of Amazon deforestation. The meridional change is not shown. The inner circulation is an anomaly due to deforestation.

The above hypothesis appears to provide a reasonable explanation for the GCM results. This work is intended to quantify this hypothesis using a mechanistic model (we use "mechanistic model," "simple model," and "intermediate-level model" loosely and sometimes interchangeably in this work), and, at the same time, to study sensitivities to the three identified land-surface-related features: albedo, evaporation, and surface roughness length. This follows the "theoretical" approach of Charney (1975), providing a complimentary method to the mainstream GCM approach.

In section 2, the background and the description of our model are given, while the validation of our model results against climatology and ENSO anomaly is discussed in section 3. In section 4, the climatic effect of Amazon deforestation is studied, while continuous deforestation is addressed and thermodynamic analysis is performed in section 5. Finally, a summary and further discussions are given in section 6.

## 2. Development of a model for tropical climatology

### *a. Background*

Simple modeling in the Tropics has achieved great success over the last decade and a half, especially in studying El Niño/Southern Oscillation (e.g., see Cane 1992 for a review). The Matsuno–Gill type model (Matsuno 1966; Gill 1980, hereafter referred to as the Gill model, as it is popularly called) is the central dynamical framework for most of the atmospheric models that parameterize heating in terms of SST in various ways.

Though the Gill model was originally used to study the climatological Walker circulation, the majority of

[1] The zonally symmetric part is the Hadley circulation. There is some confusion in current literature concerning east–west versus north–south circulation. Of course, this distinction is somewhat artificial. We will refer to the circulation as Walker circulation when focus is on the zonal asymmetry, otherwise we will use Walker–Hadley circulation in general.

the research has been focused on anomalous flow in the Pacific. There have been only a few further modeling efforts devoted to tropical climatology. Webster (1972) used a simplified primitive equation model to study atmospheric response to prescribed heating. Geisler (1981) studied the Walker circulation. Davey and Gill (1987) modeled the tropical atmosphere with the addition of a highly simplified water budget. More recently Seager (1991) attempted to simulate tropical climatology in a self-consistent model, in which heating was internally produced by the model. The model's heating was parameterized in terms of Newtonian cooling and convective precipitation, similar to Davey and Gill. Instead of using convective parameterizations based on the convective instability of the second kind (CISK) (Charney and Eliassen 1964), in which convection is assumed to occur when there is large-scale convergence (e.g., Zebiak 1986), Seager requires the air to be buoyant relative to the environment following the views of Betts (1982) and Emanuel (1989). Despite these efforts and partial success, Seager's model did not reproduce the intensity and limited spatial scale of convergence zones.

It has been realized that a major deficiency of such models is their too simple treatment of thermodynamics. Lindzen and Nigam (1987) emphasized the importance of boundary-layer dynamics in influencing convection, though their model is mathematically similar to the Gill model. Wang and Li (1993) combined the Gill model with the Lindzen and Nigam model and used an SST-dependent convective heating. They were able to reproduce reasonably well the climatology over the tropical Pacific.

Silva Dias et al. (1983) first applied the Gill model to the circulation over South America. Their main interest was the transient response to convection on timescales of one day to a few days. DeMaria (1985) studied the steady-state response in a similar model, but with finer vertical resolution. Kleeman (1989) and Gandu and Geisler (1991) studied the topographical effects of the Andes, pointing to the significant influence of topography on low-level circulation. More recently, Eltahir and Bras (1993) used the Gill model to study the influence of deforestation on regional circulation, suggesting that the impact of large-scale deforestation on the atmospheric circulation consists of two competing effects: the response to negative change in precipitation and the response to the positive change in surface temperature.

The popularity of the Gill-type model is largely due to its simplicity and analytical wave solutions. Its success is based on the fact that latent heat release from deep convection generally maximizes at midatmosphere, so the motion largely projects onto the gravest vertical mode. However, this is apparently invalid in regions of sinking motion where no deep convection occurs. The simple link between SST and convection has recently been questioned by many researchers (Fu et al. 1994; Zebiak 1990). Adding different features to a simple model may give a better comparison with observation but will also increase the complexity of the model. A more fundamental formulation seems more straightforward.

The purpose of the present model is to start at a more fundamental level than the conventional Gill model in producing simulation of tropical climatology for the study of atmosphere–land–ocean response to the disturbance of deforestation. A simple hydrological cycle is included. Special attention is paid to the land surface, which has been largely "forgotten" in simple modeling. In this and the following section we will describe the model and use it to simulate climatology and anomalies such as ENSO.

### b. *Atmospheric model*

#### 1) Model equations

The atmospheric model is a quasi-linear, steady-state model for the entire Tropics, with vertical log pressure and horizontal spherical coordinates. The model equations are the linearized, steady-state primitive equations with linear damping:

$$\alpha U - fV = -\Phi_x - \frac{\tau^x}{z_B} \tag{1a}$$

$$\alpha V + fU = -\frac{1 - y^2}{a}\Phi_y - \frac{\tau^y}{z_B} \tag{1b}$$

$$\frac{1}{a(1 - y^2)} U_x + \frac{1}{a} V_y + e^{z/H}(e^{-z/H}w)_z = 0 \tag{1c}$$

$$\Phi_z = \frac{R}{H} T \tag{1d}$$

$$\frac{C_p H N^2}{R} w = Q, \tag{1e}$$

where subscripts $x$, $y$, $z$ denote partial derivatives with respect to $x$, $y$, $z$. Here we use log-pressure vertical coordinate $z = -H \log(p/p_0)$, where $H$ is the assumed constant atmospheric scale height; the horizontal coordinate $x = a\lambda$, where $a$ is the radius of the earth and $\lambda$ is longitude; $y = \sin(\theta)$, where $\theta$ is latitude; $U = u \cos(\theta)$, $V = v \cos(\theta)$, where $u$ and $v$ are the zonal and meridional components of the velocity; $w$ is vertical velocity with respect to the log-pressure coordinate; $z_B$ is the thickness of the boundary layer; $\Phi$ is geopotential height; and $T$ is the temperature. Here $Q$ is the heating function, including a Newtonian cooling term; $\tau^x$, $\tau^y$ are horizontal stresses at the surface; $R$ and $C_p$ are the gas constant and the specific heat of air. We adopt the following parameter values for our standard case: Rayleigh friction coefficient $\alpha = (5 \text{ day})^{-1}$; the stability of the atmosphere is represented by buoyancy frequency squared $N^2 = 10^{-4} \text{ s}^{-2}$; and $H = 8$ km.

The simulated domain covers the entire Tropics, extending to ±42°. In the vertical, the lowest layer is approximately 2 km high and represents the planetary boundary layer. The boundaries of the vertical layers are at 1000, 800, 500, and 0 mb, with two free-atmosphere layers on top of a boundary layer (Fig. 3).

At the north and south boundary, $V = 0$; at the top of atmosphere and surface, $w = 0$. So the simulated domain is essentially a closed box. Possible effects due to wave reflection at the north and south boundaries are minimized by the fact that we are concerned with a region far away from the domain boundary. The horizontal resolution is 7.5° × 4.5° at the equator (equivalent to an R15 global spectral model). The model contains the Andes Mountains in South America, blocking the boundary layer. Figure 4 shows model orography and resolution.

### 2) Parameterization of boundary-layer drag

The horizontal momentum stress at the lowest layer is estimated by the bulk aerodynamic formula:

$$\tau^x = C_D|\mathbf{v}|U \qquad (2a)$$

$$\tau^y = C_D|\mathbf{v}|V. \qquad (2b)$$

Equations (2a) and (2b) are applied to the boundary layer only. Surface roughness length is determined from BATS (Biosphere–Atmosphere Transfer Scheme; Dickinson et al. 1993) vegetation type and parameter. The drag under neutral condition is parameterized following CCM1 (Williamson et al. 1987), which originated from Deardorff (1972):

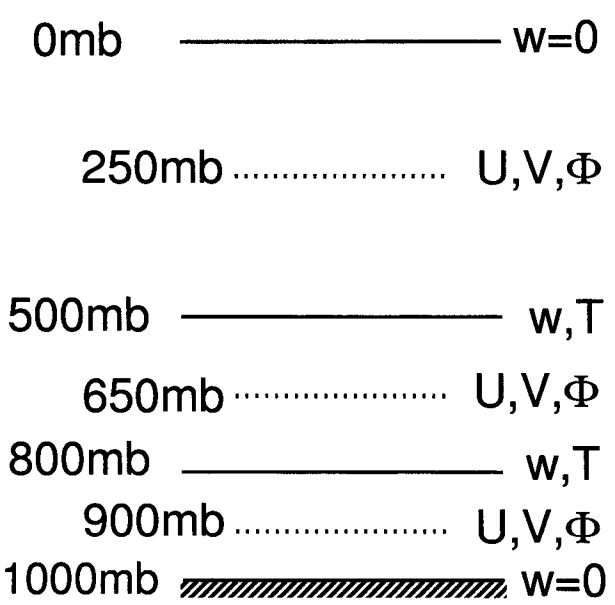


FIG. 3. Model vertical structure.

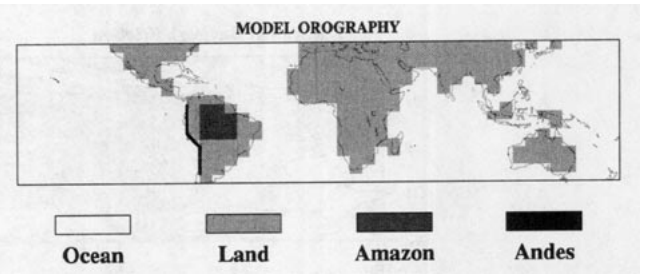


FIG. 4. Model orography. The Andes Mountains are represented by a thick black line. The Amazon is distinguished only in deforestation simulation.

$$C_{DN} = \left[k^{-1}\ln\left(\frac{0.025z_B}{z_0}\right) + 8.4\right]^{-2}, \qquad (2c)$$

where $z_B$ is boundary-layer height (about 2 km here) and $z_0$ is surface roughness length. This formulation is different from that used in high vertical-resolution models such as CCM2, in which a larger drag is applied to a much shallower layer (less than 100 m). Because of the logarithmic relationship, $C_{DN}$ computed from Eq. (2c) is slightly smaller than it would be near the surface over the ocean, but it can be as much as four times smaller over the tropical rainforest. This is an important factor to consider in Amazon deforestation simulation. The atmosphere can be quite unstable when convection occurs through the whole vertical column, over the trade wind region in the boundary layer, or over daytime desert in the lower troposphere. To account for the instability when dealing with a crude model thermodynamic treatment, we observe that similarity theory predicts that under unstable conditions the drag coefficient slowly approaches four to five times that of its neutral value, as instability becomes very large under a wide range of conditions (e.g., Arya 1988). We therefore somewhat arbitrarily set the drag coefficient $C_D$ at *twice* its neutral value everywhere:

$$C_D = 2C_{DN}.$$

Surface stresses $\tau^x$, $\tau^y$ are quadratic functions of wind velocity. The observed surface wind, instead of model wind, is used as $v$ in Eqs. (2a), (2b) (see discussion at the end of this section). The resulting "effective" Rayleigh damping in the boundary layer is then $\alpha_e = |v|C_D/z_B$, with a minimum velocity of 2 m s$^{-1}$. Figure 5 shows the calculated $\alpha_e$. Over the Pacific, it is in general agreement with the diagnosed result of Li and Wang (1994), indicating that the velocity dependence largely accounts for the spatial variation of the surface Rayleigh damping.

### 3) Parameterization of longwave radiative heating

What is most important for our purpose is the heating function $Q$:

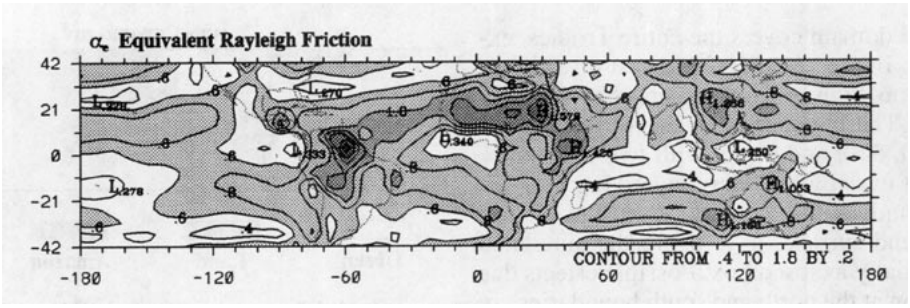


FIG. 5. Model equivalent Rayleigh friction in boundary layer. Units: $10^{-5}$ s$^{-1}$.

$$Q = Q_R + Q_C$$

with

$$Q_R = C_p(T^* - T)/\tau_R, \tag{3a}$$

where $Q_R$ is longwave radiative heating and $Q_C$ is heating due to latent heat release.

As in Davey and Gill (1987), longwave radiation is parameterized by the Newtonian cooling formula as in Eq. (3a), where $T^*$ is equilibrium temperature, $T$ is actual temperature, and $\tau_R$ is the relaxation time of atmospheric cooling or heating (heat capacity), which is normally assumed to be about 20–30 days. This value is applicable over land, where the surface adjusts quickly to solar heating. However, over ocean and on intraseasonal timescales, the SST does not respond directly to solar radiation due to its large heat capacity. On the contrary, the diabatic heating is controlled by the SST. A one-month $\tau_R$ results in a large deviation of the simulated actual temperature from the equilibrium temperature, which is taken to be the SST over the ocean and the observed surface temperatures over land in models like that of Seager (1991). Consequently, modeled temperature gradients would be much smoother than in reality. This is likely the cause of the convergence zones being too wide in Seager's model. The complex processes by which SST controls convection and radiation are not well understood and are hard to parameterize in the present model on the basis of sound physics. However, as a post priori requirement, the model-simulated temperature should not deviate too much from the equilibrium temperature over ocean. Thus, a much smaller $\tau_R$ needs to be used there. We found two days to be a good choice. Such a strong damping is perhaps more appropriate in the boundary layer due to the strong mixing there. Ambiguity always exists because of the simplicity of Newtonian cooling parameterization, especially for its linearity and locality. Over land, the cooling time is chosen to be 26 days. The atmosphere is assumed to adjust instantaneously to dry convective instability so that $T^*$ is dry adiabatic:

$$T^*(z) = T_s^* - \Gamma_d z, \tag{3b}$$

where $\Gamma_d = 9.8°$ C km$^{-1}$ is the dry-adiabatic lapse rate. Here $T_s^*$ over ocean is simply the sea surface temperature. Over land, results from previous work based on the observed surface air temperature do not seem satisfactory (e.g., Seager 1991). One reason is that the atmosphere adjusts away from this equilibrium temperature so that the modeled temperature $T(z)$ inevitably deviates from observation. Here we use the incoming solar radiation $S$ corrected by surface albedo $A$ to calculate absorbed flux:

$$F = (1 - A)S, \tag{3c}$$

where $S$ is a function of latitude only but varying with season (no diurnal cycle). In principle, one should do radiative transfer calculations to obtain an equilibrium temperature. For simplicity, we use the Stephan–Boltzman law

$$F = \epsilon\sigma T_s^{*4} \tag{3d}$$

to calculate $T_s^*$ over land, where $\epsilon$ is a somewhat arbitrary scaling constant with a value close to the emissivity of the earth as a whole. In our model, $\epsilon$ acts as a tuning parameter and is about 0.7. Such a parameterization automatically avoids the problem that high temperature artificially causes large convergence and rainfall over deserts.

#### 4) PARAMETERIZATION OF CONVECTIVE LATENT HEATING

Assuming that all the moisture is confined to the boundary layer, moisture conservation requires that precipitation

$$P = E - \frac{p_B}{g}\nabla\cdot(q\mathbf{v}_B) \tag{4a}$$

if the right-hand side is positive, and $P$ is zero otherwise. The subscript $B$ denotes the boundary layer, $E$ is evaporation, $p_B$ is the boundary-layer thickness in pressure, the second term at the right-hand side is moisture convergence in the boundary layer, $g$ is gravity, and $q$ is boundary-layer specific humidity.

For a climatological simulation, the present steady-state model switches on the precipitation parameterization whenever the water budget allows

$$Q_C = \eta(z)P,$$

with $\eta(z)$ the vertical profile of convective latent heating. We adopt a typical profile that maximizes at a height $z_u = 5.5$ km following Cornejo-Garrido and Stone (1977):

$$\eta(z) \propto \cos^2\left[\frac{\pi(z - z_u)}{z_u}\right].$$

For the coarseness of the model's vertical resolution, the fine details in the above profile is not important. Term $\eta(z)$ absorbs parameters such as latent heat of condensation and column air mass. The evaluation of $Q_C$ is completed by an integral constraint that total heating equals the total latent-heat release.

Tropical low-level relative humidity is observed to be mostly between 65% and 85%. We therefore approximate boundary-layer humidity $q$ by its saturation value $q_s$ at the lowest level:

$$q = q_s[T^*(900 \text{ mb})].$$

Neelin and Held (1987) have demonstrated the plausibility of parameterizing specific humidity in terms of surface temperature. Our result is largely similar to theirs (Fig. 6i). For an evaporation parameterization, such neglect of air dryness has only a small effect in the Tropics, where moisture is abundant and can be somewhat compensated for by a general scaling (e.g., Priestly and Taylor 1972). Employing the bulk transfer formula

$$E = 1.5\beta\rho C_W|\mathbf{v}|(q_{ss} - q),$$

where $\beta$ is surface wetness, $\rho$ is air density, $q_{ss}$ is surface saturation specific humidity, and $C_W$ is a moisture-transport coefficient taken to be the same as $C_D$. A 1.5 scaling factor is used everywhere. As in the computation of surface stress, over the ocean observed surface wind is used for $\mathbf{v}$, but with a minimum value of 4 m s$^{-1}$. Over land, 2 m s$^{-1}$ is used everywhere. Term $\beta$ is 1 over the ocean and a function of precipitation over land:

$$\beta = \begin{cases} 1 & \text{ocean} \\ P/P_0 & \text{land,} \end{cases} \tag{4b}$$

with an upper and lower limit over land:

$$0.2 < \beta < 1,$$

where $P_0$, a characteristic precipitation, is taken to be 7 mm day$^{-1}$. Such a high-precipitation rate (close to the annual average of Amazon precipitation) corresponds well to that of tropical rain forests, where water vapor is supplied at nearly the potential rate through highly efficient evapotranspiration (Shuttleworth 1988). Below this value, the functional relationship between wetness and climatological precipitation is extremely complex. It may well be nonlinear and vary from place to place and can be confidently assessed only by a comprehensive land–surface model. Here we simply adopt a linear relation. The lower limit reflects the fact that an area is never completely dry, not even a desert. One effect of imposing a lower limit is that precipitation is less than evaporation for regions where moisture convergence is negative with a smaller magnitude than evaporation (e.g., see Fig. 14a at high albedo values, which will be discussed later). This implies a negative runoff in the long-term climatological sense and appears to be unrealistic. However, on seasonal timescales, observation shows an excess of evaporation over precipitation for semidesert regions (e.g., Sellers 1965), and the extra moisture comes from soil moisture storage derived from a previous rainy season. Our model results show this excess is small and in a reasonable range.

The above formulation mimics the behavior of a bucket model in steady state. However, the evaporation calculation is not quite self-consistent: $q_{ss}$ and $q$ should be functions of model-produced temperature $T_s$ instead of $T_s^*$. Term $E$ should also be a function of model-produced wind speed. Over a nonprecipitating region, humidity and evaporation should adjust to a state where moisture divergence exactly balances evaporation as in Davey and Gill (1987). This requirement does not influence the precipitating region except at the precipitating–nonprecipitating boundary, where moisture convergence may change somewhat due to humidity change. While all of the above apparently more realistic methods could be easily incorporated into the present model, tests have shown that, given more freedom, the model can have a "climate drift" problem. Some fields over some regions become worse while others improve (probably by coincidence) in comparison with observation. However, the drift is within the range of tolerance provided the model does have some room for tuning. We choose to have less freedom so that we can single out the major mechanisms in the deforestation simulation without excessive complications.

In summary, the heating term in Eq. (1e) is parameterized as

$$Q = \frac{C_p(T^* - T)}{\tau_R} + \eta(z)H[1.5\beta\rho C_W|v|(q_{ss} - q) - (p_B/g)\,\nabla\cdot(q\mathbf{v}_B)], \tag{5}$$

where $H[x]$ is a modified Heaviside stepfunction: $H = x$, if $x > 0$; $H = 0$ otherwise. Terms $T$, $\beta$, $\mathbf{v}_B$ are model-determined, and such a parameterization makes the whole set of equations nonlinear. Table 2 summarizes some of the important parameterizations.

### c. Ocean model

An extremely simple mixed layer ocean model is used to simulate anomalous ocean temperature:

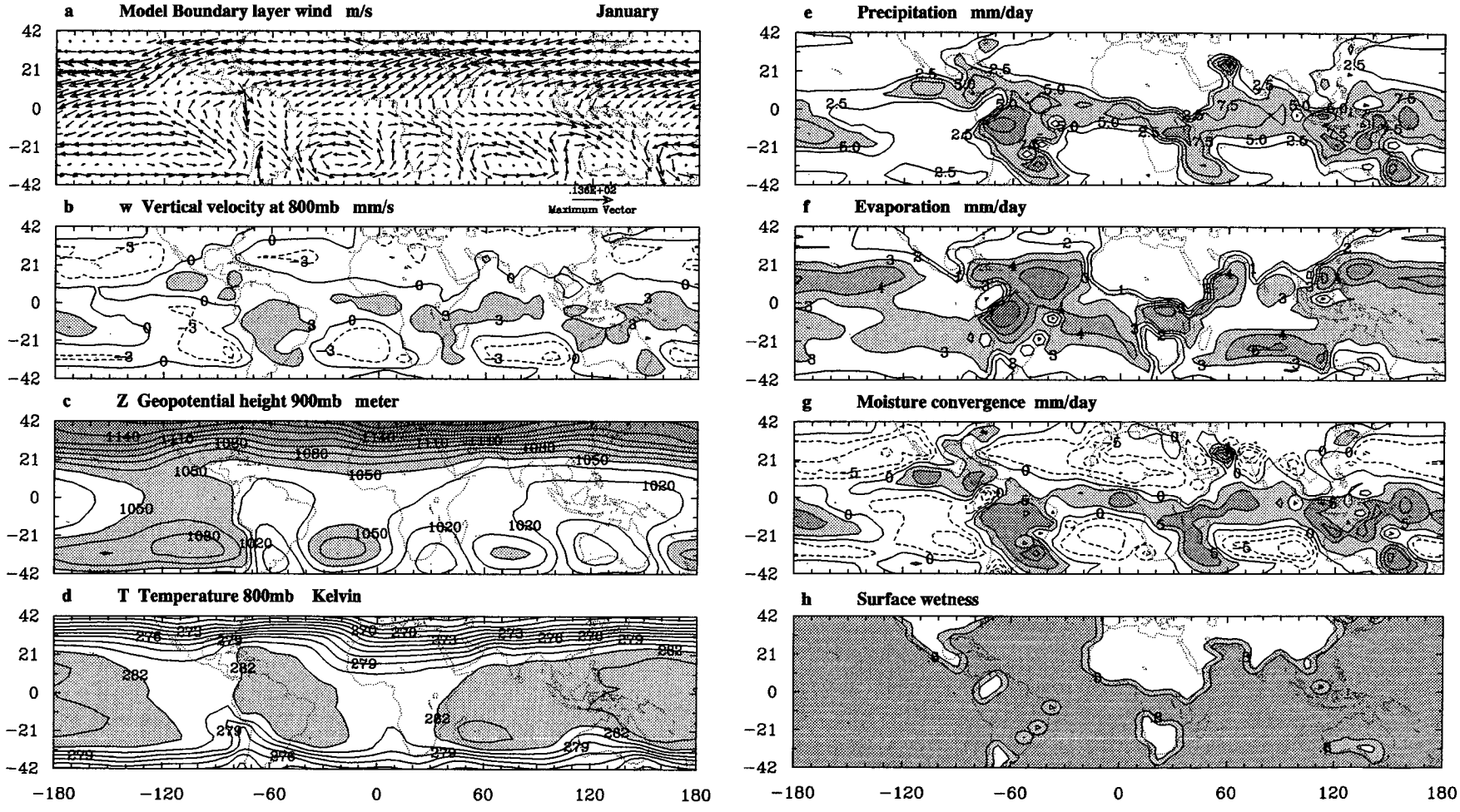
a Model Boundary layer wind m/s
January
1.36E+02
Maximum Vector
b w Vertical velocity at 800mb mm/s
c Z Geopotential height 900mb meter
d T Temperature 800mb Kelvin
e Precipitation mm/day
f Evaporation mm/day
g Moisture convergence mm/day
h Surface wetness
42
21
0
-21
-42
-180
-120
-60
0
60
120
180

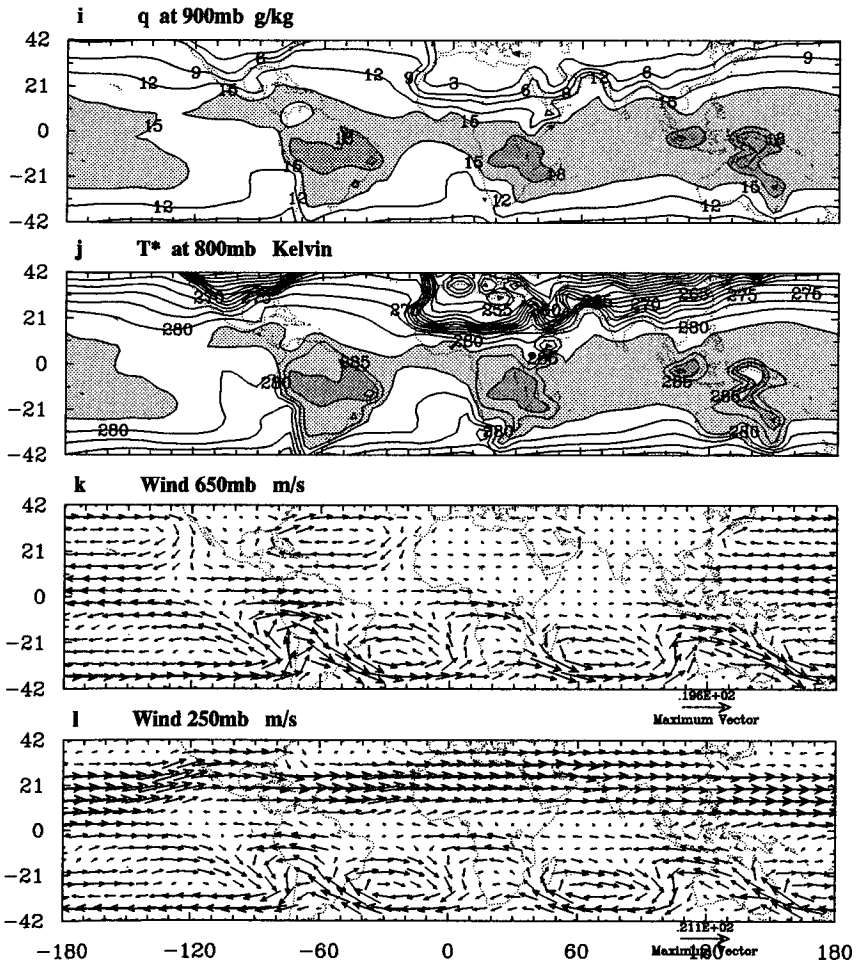


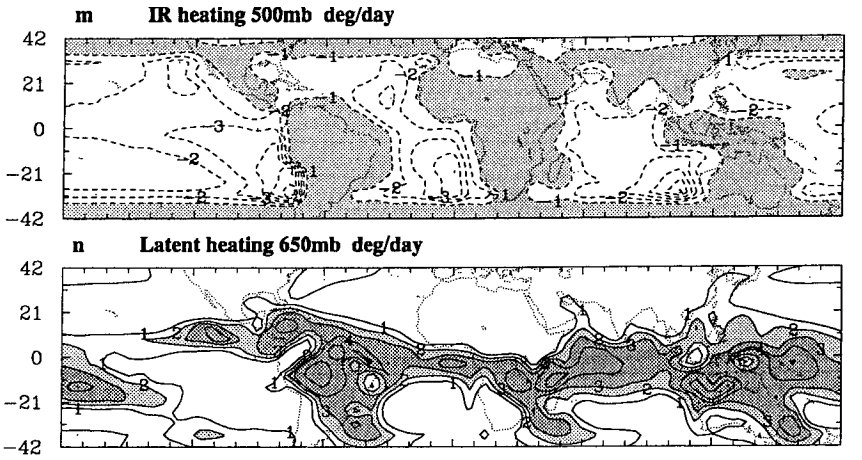


FIG. 6. Model January climatology.

TABLE 2. Important parameterizations of the atmospheric model.

| | | |
|---|---|---|
| Surface drag | $C_D = 2C_{DN}$ | $C_{DN}$ from BATS/CCM1; doubled for instability |
| Longwave radiation | $Q_R = C_p(T^* - T)/\tau_R$ | $\tau_R$ = 26 days, over land; $\tau_R$ = 2 days, over ocean |
| Equilibrium temperature | $T^*(z)$ | Solar insolation corrected by albedo + Stephan–Boltzman law to give $T_s^*$; dry adiabatic lapse rate |
| Convective heating | $Q_C = \eta(z)P$ | Water budget |
| Evaporation | $E$ | Bulk transfer formula; precipitation dependent wetness over land |
| Moisture convection | $-\nabla\cdot(qV_B)$ | Boundary layer only |

$$\alpha_0 u - fv = -g'h_x + \tau^x \frac{\rho}{(\rho_w D)} \tag{6a}$$

$$\alpha_0 v + fu = -g'h_y + \tau^y \frac{\rho}{(\rho_w D)} \tag{6b}$$

$$\alpha_0 g'h + c^2(u_x + v_y) = 0 \tag{6c}$$

$$\mathrm{SST}a = Kh, \tag{6d}$$

where $h$, $u$, $v$ are the anomalous thermocline depth and ocean current, $D$ is the average thermocline depth, $\rho$ and $\rho_w$ are the densities of surface air and of water, $\alpha_0$ is Rayleigh damping and the height damping coefficient, $c$ is Kelvin wave speed, SST$a$ is a sea surface temperature anomaly, and $K$ converts thermocline depth to surface temperature and is basically a coupling constant between atmosphere and ocean. Equation (6d) is a diagnostic relation, so thermocline height $h$ can be related to SST$a$, which in turn feeds into the atmosphere. The surface wind stresses $\tau^x$, $\tau^y$ are surface wind stresses evaluated from Eq. (2) of the atmospheric model. Following Philander (1990) and Hirst (1986), we adopt the parameter values listed in Table 3.

Such a steady-state ocean requires a nonzero Newtonian cooling coefficient for nontrivial solutions to exist. The time-dependent version of the above equation has been used extensively in modeling ENSO (e.g., Hirst 1986). The steady-state solution is not a very good approximation to reality (Philander 1990). Nevertheless, in our simulation (not shown) the model does appear to be able to simulate eastern and equatorial upwelling in both the Atlantic and the Pacific reasonably well, as driven by the observed wind or by its anomaly, although the strength and details of the pattern are questionable.

TABLE 3. Parameters used in the ocean model.

| Parameter | Symbol | Value |
|---|---|---|
| Reduced gravity | $g'$ | 0.02 m s$^{-2}$ |
| Mean thermocline depth | $D$ | 100 m |
| Kelvin wave velocity | $c$ | 1.4 m s$^{-1}$ |
| Rayleigh and Newtonian coefficient | $\alpha_o$ | $10^{-7}$ s$^{-1}$ |
| Coupling constant | $K$ | 0.03° C m$^{-1}$ |
| Density of surface air | $\rho$ | 1.2 kg m$^{-3}$ |
| Density of water | $\rho_w$ | $10^3$ kg m$^{-3}$ |

### d. *Input data and numerical method*

The January SST climatology of the Climate Analysis Center (Reynolds 1988) is used as our surface equilibrium temperature $T_s^*$ over the ocean. Over land, incoming solar radiation at the top of the atmosphere is calculated using the theoretical astronomical formula of Sellers [1965; Eq. (3.7)], in which the solar declination angle is the only parameter to vary with the day of year. The ERBE [(Earth Radiation Budget Experiment; Ramanathan et al. (1989)] satellite-observed, clear-sky albedo is used as the albedo $A$. Since the scaling constant $\epsilon$ in Eq. (3d) is somewhat tunable, the correspondence of this albedo to the real planetary albedo is not important. Equation (3c) is then used to calculate the solar radiation absorbed by the land-surface $F$, which is a function of latitude (but not longitude, because the model has no diurnal cycle). The equilibrium surface temperatures calculated by Eq. (3d) are smoothed somewhat, so they merge with ocean temperatures smoothly. Term $T^*(z)$ is obtained from Eq. (3b) and then serves as the driving force for the model according to Eq. (3a).

Finite-difference methods are used for the numerical solution of the governing equations, that is, Eqs. (1a)–(1e) in combination with Eq. (5). A sparse matrix technique based on LU decomposition of matrix and a very efficient iteration procedure are utilized. More details of the mathematical techniques are given in the appendix.

## 3. Modeled climatology and ENSO anomaly

### a. *January climatology*

Simple models are sensitive to a number of parameters and therefore leave much room for tuning. The present model strives to base the parameterization on sound physics and to constrain the parameter range to

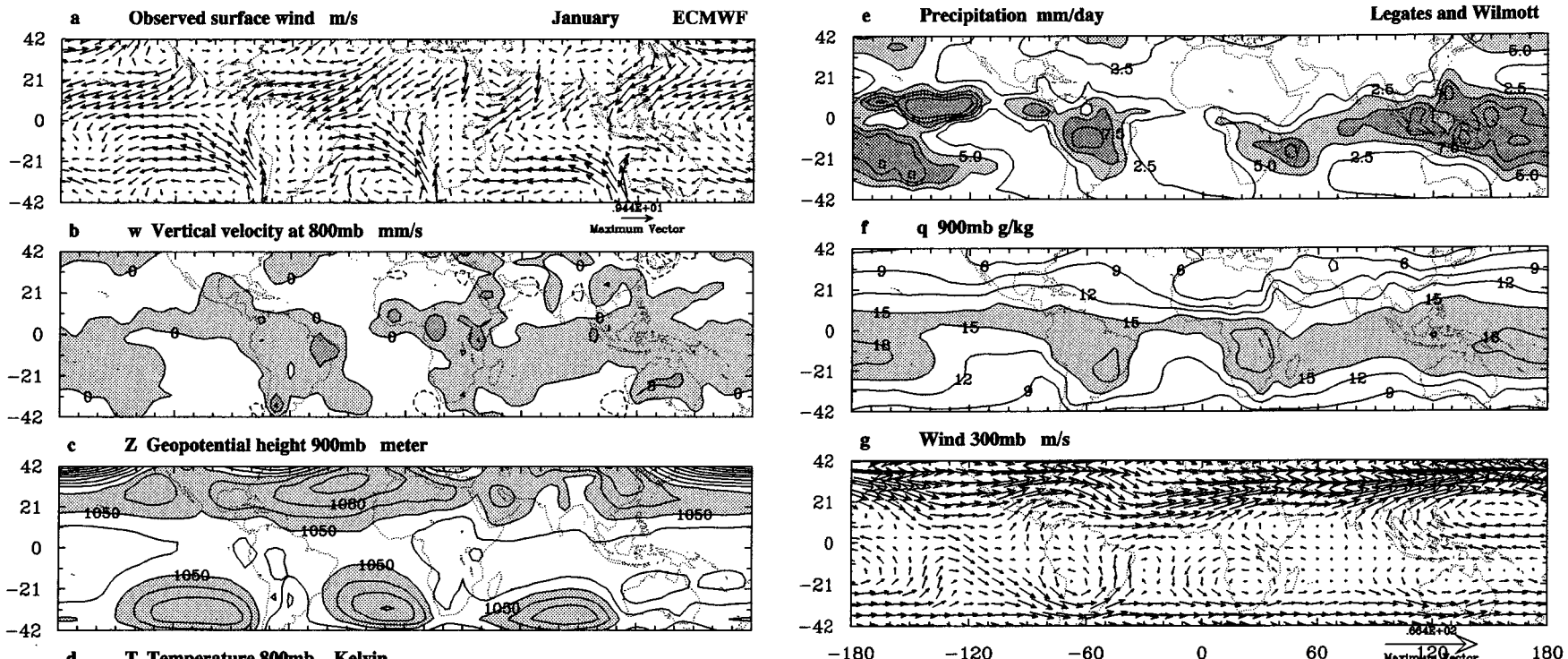


FIG. 7. Observed January climatology. From ECMWF analysis except precipitation from Legates and Wilmott (1990).

be physically acceptable. Input data are very few. The model internally determines convergence and associated latent heating, and it automatically responds to land-surface perturbation, such as albedo change. Such a self-consistent model is essential for studying climate change, such as that due to deforestation.

The model January climatology is shown in Fig. 6, while that observed is shown in Fig. 7. Note that there are fewer panels in Fig. 7 than in Fig. 6 because the number of the archived fields from observational data is limited. In particular, evaporation and surface wetness are poorly observed and not available to us. Comparing Fig. 6a with Fig. 7a, it is seen that, overall, the wind and its convergence field look quite realistic. The trade winds have the proper magnitude and direction. The equatorial westerlies off the west coasts of Panama and Central Africa and over the Indian Ocean are reproduced. Comparing Fig. 6b with observation in Fig. 7b, the South Pacific convergence zone (SPCZ) and the Pacific intertropical convergence zone (ITCZ) have the right strength and spatial extension. The southern Amazon develops its summer maximum convergence. The convergence over Africa and the west Pacific warm pool are produced. A relatively unrealistic feature is the following: off the Central American coasts, the convergence is somewhat too strong as a result of the local SST maxima because model convergence is directly linked to surface temperature through Eq. (1e). This is a fundamental limitation of this kind of treatment of thermodynamics, in which heating is instantaneously and solely balanced by adiabatic cooling of upward motion. There is some ambiguity in terms of convergence comparison, because the observation is the climatological mean of transients on a wide range of timescale, whereas the model has only one steady state. Due to the smoothness of the humidity field, the model wind convergence is tightly related to the moisture convergence, which is in turn directly associated with the model precipitation. In reality, as a result of the variation of the humidity with time, the wind convergence can be quite different from moisture convergence.

The boundary-layer moisture convergence pattern in Fig. 6g is similar to wind convergence (see Fig. 6b) because the moisture field is much smoother than wind, as demonstrated by comparing Fig. 6i with Fig. 6a or by comparing Fig. 7f with Fig. 7a. However, small differences do show up as the result of moisture advection. The modeled moisture field in Fig. 6i is close to the observational one in Fig. 7f, in agreement with the results of Neelin and Held (1987). For evaporation, there is a lack of good observation for comparison. The modeled evaporation in Fig. 6f appears to be reasonable. Trade wind regions have large evaporation due to consistently strong winds there. The large evaporation over the Amazon and central Africa is linked to the large drag of the forest. The modeled surface wetness (Fig. 6h) captures the large-scale wetness pattern over land, losing some fine spatial variation, partly due to the high and low cutoffs in the parameterization [Eq. (4b)]. The precipitation in Fig. 6e compares favorably with observation in Fig. 7e. The west Pacific warm pool and extended SPCZ rain at the right amount. The southern Amazon develops a winter maximum, while the northern Amazon is in its dry season. This is the direct result of solar insolation, and the southern maximum is also partly due to the large evaporation there. Again the problem of convergence is also reflected in precipitation, namely, too much rain around Central America.

The geopotential height pattern in Fig. 6c appears to be in good agreement with observation in Fig. 7c. This field can only be determined up to a constant difference by the model. An equatorial trough runs across the entire globe, with a low in northeastern Australia and local minima to the south of the Amazon and southern Africa. Subtropical highs are well reproduced in the Southern Hemisphere, which is at its summer, and, accordingly, midlatitude westerly winds are produced. This is probably the right answer for the wrong reasons: no forcing is applied outside 30° latitude, and the model domain boundary is not too far away. The winter hemisphere subtropical highs are less well defined.

In light of the good simulation of geopotential height, the modeled temperature field in Fig. 6d is not as good, but the overall pattern is still within a reasonable range in comparison with Fig. 7d. Due to the large Newtonian coefficient used, the temperature over the ocean is not far from equilibrium temperature, which can be seen by comparing Fig. 6d with Fig. 6j. We noticed that the model appears to have a tendency to produce two local temperature maxima astride a major convergence zone. Such local warm cores are prominent over land in the observations (better seen in Newell et al. 1972), and they cannot be always easily explained by surface warming above deserts. Interestingly, a zonally symmetric version of the present model shows these local maxima sitting between tropical rising regions and subtropical sinking regions, and it is closely linked to the vertical latent heating profile used. This finding deserves further study.

What is perhaps the most unrealistic and worrisome feature in the model boundary layer is the overly strong westerly winds west of the major convergence zones: the Amazon, central Africa, and the Pacific warm pool, as can be seen from Fig. 6a. Such strong westerlies are typical of the Gill model as a manifestation of equatorial Rossby waves, whose wave speed is one-third that of the Kelvin wave. In fact, the dynamics in Eq. (1a) imply the vanishing of the zonally averaged zonal velocity at the equator. In reality, easterlies dominate over westerlies along the equator. Thus, modeled westerlies are too strong, especially over central Africa where observation shows only a hint of westerly. Although Wang and Li (1993) and Zebiak (1990) found that the advection of momentum is negligible over the Pacific, it is possible that it may play a role in some

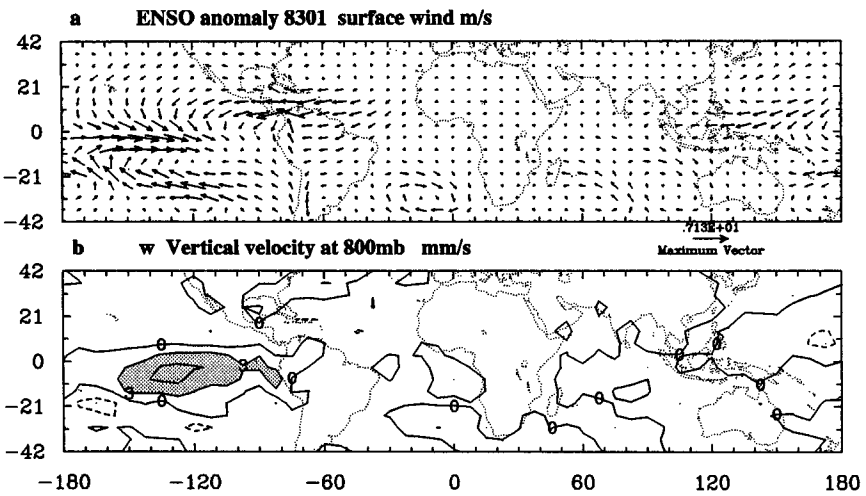


FIG. 8. El Niño anomaly of January 1983 simulated by the model.

other regions. Other candidates are the diurnal cycle and synoptic transients. This effect is alleviated over the Amazon due to the blocking of the Andes Mountains. In fact, the northwesterly wind there is similar to the well-known "jet" emanating from the Amazon basin flowing southward, though the model westerly wind has too wide a spatial extension. Similar results are obtained by Gandu and Geisler (1991) and Kleeman (1989) in simulating Amazon low-level flow response to prescribed heating.

The model 650-mb winds (Fig. 6k) are similar to observations (not shown), but the strong westerly problem is even worse than in the boundary layer, so that the equatorial Atlantic trade winds almost completely vanish. Upper-level winds (250 mb) (Fig. 6l) bear good resemblance to observed 300-mb winds (Fig. 7g) within ±20°, although some details are not in agreement. These results comply with the importance of transients in upper-tropical atmosphere that are not represented in the model.

Observations over the eastern Atlantic and western Pacific convective regions (e.g., Cotton and Anthes 1989, chapter 6) have constantly demonstrated that infrared heating is negative throughout a vertical column, while convective latent heating dominates over IR cooling. Model results (Figs. 6m,n) show the same trend. In convective regions, IR heating is generally quite small and negative. The large IR cooling in nonprecipitating regions is balanced by the adiabatic warming of descending air. The latent heating pattern follows precipitation, with 500-mb heating much stronger than at lower levels (not shown), a direct result of the vertical profile of latent heating. The magnitudes of latent heating are in a reasonable range and are generally smaller over land than over the ocean due to the large difference in Newtonian cooling time $\tau_R$. In a sensitivity study where the vertical heating profile is set flat (latent heating distributed uniformly in the vertical), IR heating in the convective region is found to be positive—an unrealistic feature. This interesting result again demonstrates the importance of the vertical-heating profile.

We have also simulated July climatology (see Zeng 1994) and annual cycle (see Fig. 12 for Amazon average). In general, July climatology is somewhat less well simulated. The monsoons are too strong due to the model's high sensitivity to surface condition. The annual pattern is well captured but Amazon is too dry in summer. See further discussion in section 4.

### *b. Simulation of ENSO*

The model is designed to simulate tropical climatology. An important test of the model would be to see how it works for anomalous boundary conditions, such as those related to El Niño/Southern Oscillation. In one model run, observed SSTs for January 1983 are used in place of climatological SSTs to drive the model. The model results are shown in Fig. 8.

The model develops strong anomalous westerlies in the central to eastern Pacific and easterly toward the western Pacific warm pool. An easterly anomaly is also seen north of the equator and east of the main convergence anomaly center (around 120°W). These are similar to what were observed (Fig. 9). The easterly anomaly north of the equator in the eastern Pacific appears to be somewhat too wide. The simulated convergence anomaly occupies most of the equatorial Pacific, but the center is somewhat too far to the east compared to the observed outgoing longwave radiation (OLR) pattern.

In general, the present model appears to better simulate winds and their convergence associated with ENSO than do anomaly models (e.g., Zebiak 1986).

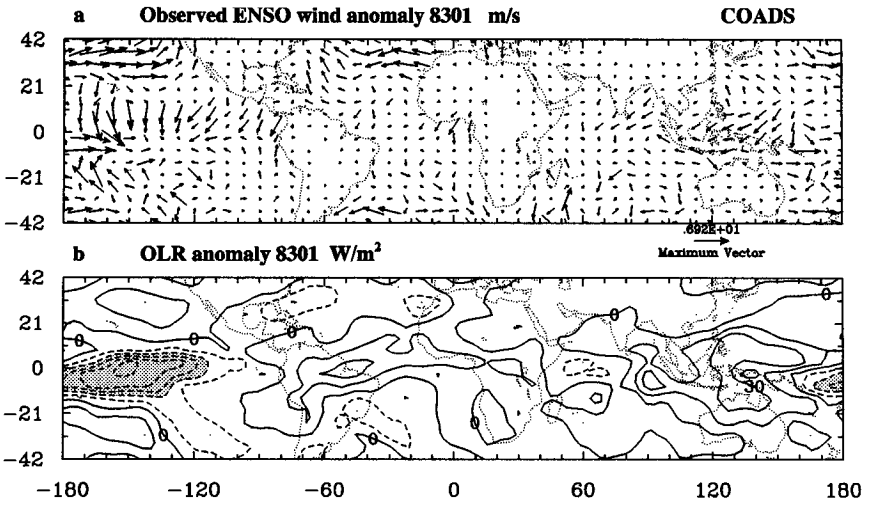


FIG. 9. Observed El Niño anomaly of January 1983.

This is expected mostly because of the nonlinear nature of air–sea interaction (Seager 1991; Zebiak 1986). It is not the anomaly but the total SST that determines the convergence and precipitation pattern. The atmosphere "feels" more of the effect of an anomaly of a warm region than that of a cold area. This model also appears to do better, in general, than simpler climatology models.

## 4. Climatic impact of Amazon deforestation—mechanism revealed by the model

### *a. The model and simulated climatology (control)*

In the previous section, we discussed model-simulated January climatology. Over the Amazon, both convergence and precipitation are well captured. In January, the southern Amazon is in its wet season, while the northern Amazon is in its dry season. While the wind field appears to be quite reasonable over the ocean, it is less realistic over the Amazon. The prominent southward "jet" out of the Amazon is present but is apparently too wide. In reality, the easterly trade winds penetrate deep into the interior of the Amazon before turning southward. The appearance of the overly strong westerlies is probably related to the neglect of nonlinear advection, which brings easterly trade winds from the Atlantic into the Amazon. As a first attempt to simulate tropical land climatology via a simple model, we will simulate deforestation, while being cautious not to expect close correspondence with reality.

The model Amazon and Andes are shown in Fig. 4. In the following discussion, averages of various fields refer to the area average over the model Amazon.

The modeled January climatology is referred to as the control run. In the control run, average precipitation over the region is 8.9 mm day$^{-1}$ while evaporation is 4.9 mm day$^{-1}$, which contributes 55% to the total precipitation (thereafter any percentage is in reference to the control precipitation, which is 100% unless otherwise specified). The other 45% comes from moisture convergence. These are in good agreement with observation (Salati 1987). Many GCM simulations have a slightly larger percentage of evaporation (e.g., see Fig. 15, which will be discussed later).

GCM simulations and theoretical consideration have so far pointed to three factors with major influence on regional climate: albedo, evaporation, and surface roughness length. Among the three, albedo and roughness length are boundary conditions and can be changed in a straightforward way in the model. However, evaporation depends on many processes and is itself a result of land–atmosphere interaction. We choose to deal with it instead of, say, soil moisture (Sellers 1992), from an atmospheric point of view. In this section, the three factors are studied in the context of the present model.

### *b. Albedo increase (A5, A5_fixEq)*

In experiment A5, the Amazon region albedo $A$ is increased by 0.05 (this corresponds to about −3°C in $T^*$; note the initial albedo is not necessarily the same everywhere, and a change of 0.05 in albedo is at the lower side of various GCM experiment assumptions) without any other change to the model. Figure 10 shows the difference fields (deforestation − control). Apparently, a sinking motion anomaly has developed over the deforested area, accompanied by an increased low-level pressure and westerly outgoing flow anomaly emanating from the Amazon to the Atlantic. Interestingly, the Andes do not completely block the interaction between the Amazon and the eastern Pacific, though the barrier extends up to the top of the boundary

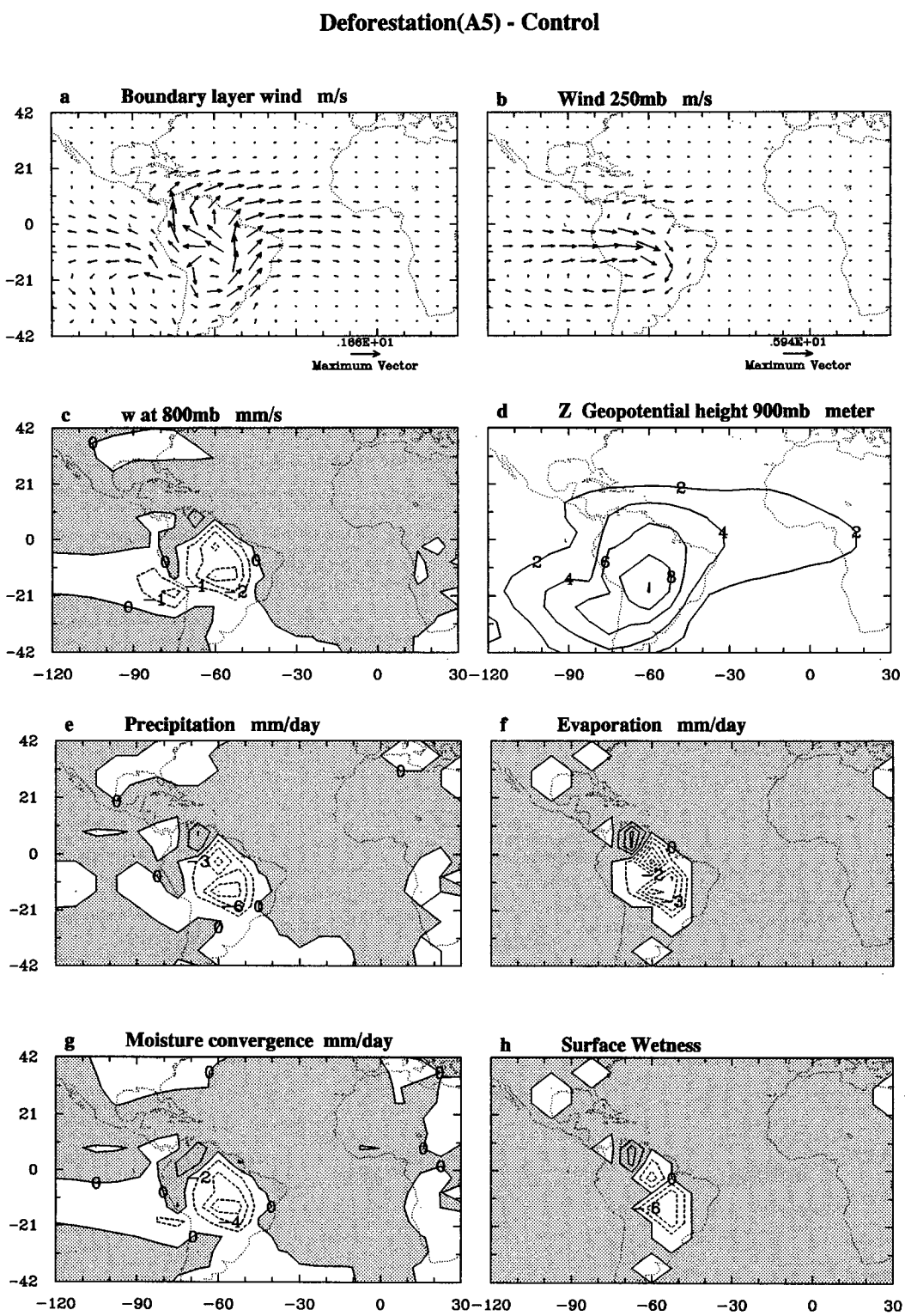


FIG. 10. Consequences of Amazon deforestation in January simulated by the model. Shown is the difference between experiment A5 (albedo increased by 0.05) and the control.

TABLE 4. Modeled January Amazon water budget.

| | Control | Deforestation − control | | | |
|---|---|---|---|---|---|
| | | A5 | A5_fixEq | WET70 | ROUGH2 |
| Precipitation | 8.9 (100%) | −5.0 (−56%) | −1.1 (−12%) | −3.1 (−35%) | −0.1 (−1%) |
| Evaporation | 4.9 (55%) | −2.3 (−26%) | 0 | −2.0 (−22%) | 0.0 |
| wetness change only | | −1.9 (−21%) | | | |
| humidity change only | | −0.7 (−9%) | | | |
| nonlinear term | | +0.3 (+4%) | | | |
| Moisture convergence | 4.0 (45%) | −2.7 (−30%) | −1.1 (−12%) | −1.1 (−13%) | −0.1 (−1%) |
| wind change only | | −2.5 (−28%) | | | |
| humidity change only | | −0.5 (−5%) | | | |
| nonlinear term | | +0.3 (+3%) | | | |
| Wetness | 0.88 | −0.36 | −0.01 | −0.36 | −0.01 |

Unit is millimeter per day except wetness, which is dimensionless.
Deforestation experiments:
A5 is albedo increased by 0.05;
A5_fixEq is albedo increased by 0.05, evaporation and humidity are held as in control;
WET70 is wetness 70% of computed value;
ROUGH2 is surface roughness is that of grass, pure dynamic effect.

layer. Both pressure and vertical velocity anomalies cover the whole Amazon and extend slightly outward onto the surrounding areas as a result of smoothing and large-scale response. Surface geopotential height has decreased by as much as 10 m (about 1 mb in surface pressure). Such a decrease in surface pressure gradient along the equator from the Amazon to the Atlantic largely counterbalances the original pressure gradient and results in the near vanish of the zonal pressure gradient force and zonal wind along the equator (not shown). The overall anomaly pattern is very similar to the typical Gill-model response to an off-equator heat source (Gill 1980), except that the sign is reversed. The wind anomaly corresponds to a weakened Hadley–Walker circulation, in accordance with our speculation in the introduction. Temperature decreases by about 1°C (not shown), which is smaller than the decrease in $T^*$ [due to albedo increase, Eq. (3)], resulting in a decrease in boundary-layer IR heating.

Precipitation over the Amazon is reduced by 56%, of which evaporation contributes 26% while moisture convergence contributes 30% (Table 4). The spatial pattern indicates that the northern Amazon in its dry season suffers most from deforestation, in relation to its drier winter climate. It is interesting to note that while decreases in evaporation are relatively localized, the convergence anomaly is more homogeneous and spatially spread out because the model's large-scale dynamical response is determined by not only the scale of heating, but also by the equatorial radius of deformation.

Accompanying the drying over the Amazon, the surrounding areas except to the south generally have an increase in precipitation, evaporation, and moisture convergence. Some researchers refer to this as a "dipole" pattern. The mechanism is straightforward in the present model: a cold anomaly in the deforested region induces anomalous sinking air, which is compensated for by rising air in the surrounding area. Such reasoning has been invoked to explain GCM results; however, it is probably more appropriate, because of nonlinearity, to think of this situation in terms of the total field instead of the anomaly. For instance, southeastern Brazil receives substantial amounts of solar radiation but less than the Amazon region, so it cannot compete with the Amazon in inducing convergence. After deforestation, southeastern Brazil receives relatively more solar energy (higher $T^*$) and attracts more convergence. This type of anomaly versus total-field interpretation has been encountered in ENSO observations and simulations (Zebiak 1986). A decrease in precipitation to the south of the Amazon can be attributed to the weakening of the jet, which brings in less moisture after deforestation.

The moisture budget averaged over the model Amazon is listed in Table 4. For better insight, the change of precipitation can be broken down into contributions from various branches (one of the strengths of a simple model), namely, evaporation and moisture convergence. The former includes contributions from wetness and the saturation specific-humidity slope, and the latter includes the contributions from specific humidity and wind convergence. The individual contributions are calculated by holding the other term in multiplication as in the control run (e.g., when computing the contribution to moisture convergence of wind $v_B$ only, humidity $q$ of the control run instead of that of deforestation is used). Since the changes are relatively small, the nonlinear interaction of two factors is expected to be small and is computed as a residual.[2] Then

[2] Consider $\alpha, \beta \ll 1$, then $(1-\alpha)(1-\beta) = 1 - \alpha - \beta + \alpha\beta \approx 1 - \alpha - \beta$, where $\alpha\beta$ is a second-order quantity. The result here is slightly more complicated due to the gradient operator and spatial averaging. See Stein and Alpert (1993) for a more complete discussion.

the changes of various parts of the Amazon water budget due to deforestation are (mm day$^{-1}$, also listed in Table 4):

$$\text{precipitation}(-5.0)\begin{cases}\text{evaporation}(-2.3)\begin{cases}\beta(-1.9)\\ q_{ss}-q(-0.7)\\ \text{nonlinear}(+0.3)\end{cases}\\ \text{convergence}(-2.7)\begin{cases}\mathbf{v}_B(-2.5)\\ q(-0.5)\\ \text{nonlinear}(+0.3).\end{cases}\end{cases}$$

Since $q_{ss} - q$ is a function of $T^*$ and thus a function of solar radiation $S$ only, one can interpret that less evaporation ($-0.7$ mm day$^{-1}$) is partly a direct result of less available solar energy at higher albedo. However, this effect is small compared to that due to a drier surface ($-1.9$ mm day$^{-1}$). As indicated by Eq. (4b), wetness decreases linearly with precipitation below 7 mm day$^{-1}$. Drying as a result of less precipitation is the major factor, especially in the already "dry" region. For moisture convergence, the contribution from lower humidity $q$ as a direct result of smaller $T^*$ is almost negligible ($-0.5$ mm day$^{-1}$). The change in large-scale circulation, namely, the changing wind convergence, plays a key role ($-2.5$ mm day$^{-1}$).

To summarize, reduction in albedo over the Amazon reduces heating in the atmosphere above and results in a weakened Walker–Hadley circulation with less convective precipitation. The resultant drying, in turn, gives out less evaporation, thus further reducing precipitation and convergence. This positive feedback loop eventually results in a much weakened Atlantic Walker–Hadley circulation and a substantially weakened hydrological cycle.

To further demonstrate the importance of the positive feedback loop, in experiment A5_fixEq, evaporation and humidity are held everywhere the same as in A5; therefore, reduction of absorbed solar energy affects only $T^*$ and the wind. The precipitation is then reduced only by 12% (Table 4), much less than the 56% in A5. This difference is solely due to changes in moisture convergence, which is only about one-half of the moisture convergence in the A5 case.

### c. *Evaporation change only (WET70)*

Dirmeyer (1992) found in a GCM study that albedo change is the sole factor responsible for reduced precipitation. Since a deforested surface cannot supply as much moisture, due to the smaller water-holding capacity of its soil, smaller canopy and air conductance, etc., this result seems surprising. In this experiment, we group all the possible changes into a lower wetness by artificially reducing the wetness factor $\beta$ by 30% after the computation of Eq. (4b), while keeping it the same function of precipitation. Nothing else is changed. The anomalous spatial pattern is largely similar to A5. The average model precipitation is reduced by 35%, with 22% from evaporation decrease and 13% from decrease in moisture convergence. However, our simple model does not have the diurnal cycle thought to be responsible for the GCM result.

### d. *Effects of surface roughness length (ROUGH1, ROUGH2)*

One consequence of smaller roughness length is less evaporation and thus a warmer surface. The model does not have a surface energy balance constraint, and less evaporation does not lead to a warmer surface. Thus, the present model is incapable of assessing the important issue of disturbance to surface energy. However, its dynamical effect can be partially explored. In experiment ROUGH1, the roughness length over the deforestation area is reduced to that of grass. This corresponds to about twice as small a drag coefficient $C_D$. This result is different from Sud et al. (1995), where $C_D$ has a four-fold decrease due to the different parameterization used (see section 2). Since it is proportional to $C_D$, the evaporation after deforestation is only about one-half of that in the control case. As the feedback loop works, the precipitation is reduced by 51% (not shown in Table 4). Considering that model parameterization of evaporation ignores complex processes of evapotranspiration through soil and vegetation and the availability of solar energy and moisture, this number appears to be too large. However, it points to the fact that smaller roughness length reduces the efficiency of moisture being transported from soil and vegetation into the atmosphere. This effect may be more appropriately categorized as evaporation change.

By using the same drag as in the control for the parameterization of evaporation, the pure dynamical effect of roughness length change is studied (ROUGH2). The difference fields in Fig. 11 show a peculiar wind anomaly centered on the equator, with a negligible convergence anomaly (also Table 4). This pattern is intriguing and hard to explain. In general, the wind becomes stronger in a deforested area, similar to what was found by Sud et al. (1995). We can understand the model behavior in terms of Ekman pumping. Using Eqs. (1a), (1b), (2a), (2b) and ignoring Rayleigh damping, we have for boundary layer:

$$\nabla \times (C_D \mathbf{v}) = \sigma w_1,$$

where $w_1$ is the vertical velocity at the top of the boundary layer (800 mb), and $\sigma$ absorbs other coefficients. Provided $w_1$ does not change with a two-fold decrease in $C_D$, one way to satisfy the Ekman relation is to have a two-fold increase in wind velocity, so the term in the bracket of the above equation has the same values. This appears to be largely what the model does. The negligibly small change in $w_1$ is probably an artifact result-

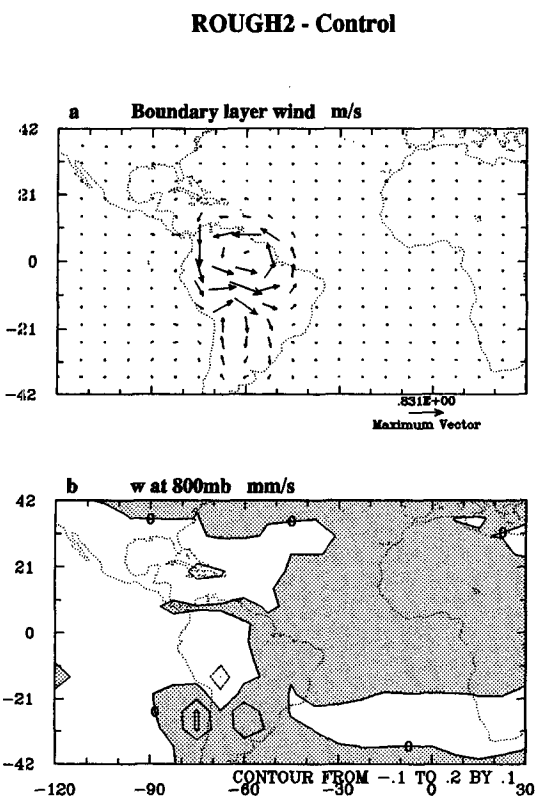


FIG. 11. Dynamical effect of reduced roughness length over the Amazon in January.

ing from the model's overly simplified treatment of the thermodynamic equation, in which the convergence is highly sensitive to thermodynamic factors but probably too insensitive to dynamical change. In a more realistic model, such a significant change in wind field would likely result in a change in moisture convergence. Further study and understanding of this is needed.

As mentioned in footnote 2, the combined effect of two factors consists of three parts, that is, the individual contributions and the contribution due to the nonlinear interaction between the two factors. If the latter contribution is small, at least to a first-order approximation, the combined effect is simply the superimposition of the effects of individual factors. Our simulations with more than one factor (results not shown) demonstrate that the effect due to the nonlinear interaction of factors is indeed small.

### e. Annual cycle

Figure 12 shows the model-simulated annual cycle of precipitation, evaporation, and moisture convergence averaged over the model Amazon. The overall trend is largely similar to the observation and GCM results (e.g., see Fig. 2 of Dickinson and Kennedy 1992). Maxima in the above three fields during spring and fall basically reflect the solar-heating maximum around the equator at the time of the year. In northern summer, North America develops an unrealistically strong "monsoon" that attracts much of the moisture (Zeng 1994) and leaves the Amazon completely dry. The nonzero evaporation in southern winter is due to the imposed lower limit in surface wetness [Eq. (4b)]. In general, the modeled annual cycle for both control and deforestation has a larger amplitude than its GCM counterpart, partially reflecting the model's overly high sensitivity to solar heating. Another factor is that the model's monthly climatology is created by running toward steady state under perpetual solar radiation, in contrast to the seasonal marching in the real world.

### f. Impact of deforestation on ocean

In the introduction, we have speculated that a weakened Walker circulation and trade wind would cause a decreased SST gradient over the Atlantic, and that this, in turn, might feed back into the loop positively. We therefore employed the simple mixed-layer ocean model (bounded by realistic continents) to study the feedback.

In the coupled run, the control model climatological surface wind is set to correspond to observed SST over ocean and $T_s^*$ over land. The deforestation (A5) total wind is then used to calculate the SST anomaly using the ocean model, and this SST anomaly is then added to the SST climatology, which, in turn, is used in the atmospheric model to produce a new surface total wind. This procedure is executed only a few times before the coupled model converges to an equilibrium state.

Figure 13 shows that the Atlantic SST does change as expected, with about 1°C anomalous gradient across the basin. The magnitude, of course, depends on the coupling strength. For instance, west Atlantic should be less sensitive than the east because of the deeper

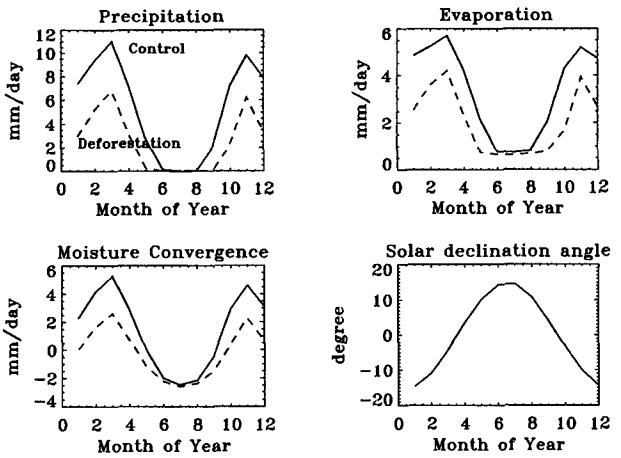


FIG. 12. Modeled annual cycle of Amazon hydrology. Solid line: control; dashed line: deforestation. Unit: millimeters per day.

thermocline depth there. Interestingly, the eastern Pacific SST gradient has strengthened somewhat, driven by outgoing flow from the Amazon despite the blocking of the Andes. However, the influence hardly goes beyond the central Pacific. Comparison between this run and one without feedback from ocean shows that the small change in SST has only a negligible effect on the atmosphere, as expected, because that is a higher-order effect compared to the deforestation change. However, a cooling in SST in the west Atlantic may affect the land–sea-breeze characteristics, which can influence coastal Amazon. Detailed analysis of the interaction among the ocean, atmosphere, and land surface (change) is beyond the scope of this paper.

## 5. Continuous deforestation and analysis of thermodynamic equation

It is interesting to ask: what would happen if the land degradation continues? What if the tropical rain forest were replaced by desert? Such theoretical questions are helpful in understanding the tropical circulation system and climatology.

In one set of model runs similar to A5, the albedo is increased over the Amazon in January continuously from no change to a 0.10 increase. Figure 14a shows the modeled precipitation, evaporation, and moisture convergence as a function of albedo change. The moisture convergence drops approximately linearly down to zero at $\Delta A = 0.085$. Evaporation decreases somewhat slower. At zero moisture convergence, the precipitation has not vanished because of the contribution from evaporation. The area averaging has some effect on the curve. As albedo increases further, convergence becomes negative while precipitation approaches zero and evaporation approaches a value limited by the model-imposed lower limit of wetness 0.2. When precipitation and convergence are plotted against evaporation in Fig. 14b, the relations are very much linear, except in the beginning they decrease at a faster pace.

In another set of runs similar to WET70, the wetness is continuously decreased from its control value to zero. Figure 15 shows that precipitation and convergence decrease almost linearly from control values to about 1 mm day$^{-1}$ as evaporation reaches zero. Thus, the present model has the property that if albedo increases to some sufficiently high value and evaporation is reduced accordingly, the tropical Amazon is able to sustain a sinking motion and maintain a dry climate. On the other hand, if only evaporation is reduced as a result of the surface condition change while albedo is fixed equal to that of a rainforest, the region is able to keep a relatively small convergence and precipitation. However, it is not clear how realistic this model response is, as discussed further in section 6.

The approximately linear relations in Figs. 14b and 15 indicate a simpler relationship among the three terms in the thermodynamic equation than the relatively complex dynamic equations and physical parameterizations. In fact, we find the thermodynamic equation is the controlling agent. For the Amazon, where air undergoes rising motion, the thermodynamic equation [Eq. (1e)] and Eq. (5) for the model boundary layer can be combined as (the variables are loosely treated as area averages)

$$\tilde{w} = (\tilde{T}^* - \tilde{T}) + E + C,$$

where the variables are dimensionalized to be millimeters per day, so we can drop all the coefficients that are not important here. This relation states that in precipitating region, diabatic heating from longwave radiation and precipitation (with contribution from evaporation and moisture convergence) is exactly balanced by adiabatic cooling from large-scale upward motion. Since change in specific humidity $q$ is quite small, moisture convergence $C$ is approximately

$$C \approx \tilde{q}\tilde{w},$$

where $\tilde{w}$ is the vertical velocity at the top of the boundary layer. Eliminating $\tilde{w}$ from above two equations, it is easy to get

$$C = C_0 + \frac{\tilde{q}}{1 - \tilde{q}} E \tag{7a}$$

and

$$P = E + C = C_0 + \frac{1}{1 - \tilde{q}} E, \tag{7b}$$

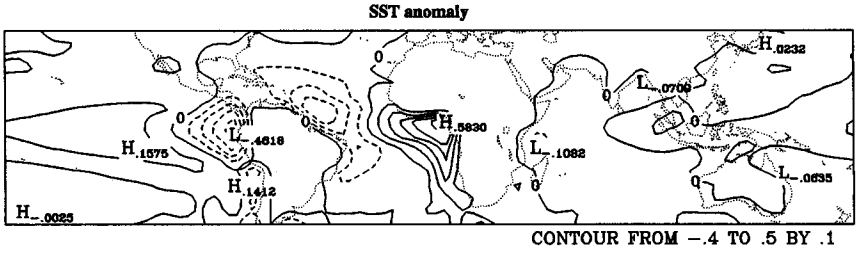


FIG. 13. SST anomaly in response to Amazon deforestation (A5). Unit: degrees Celsius.

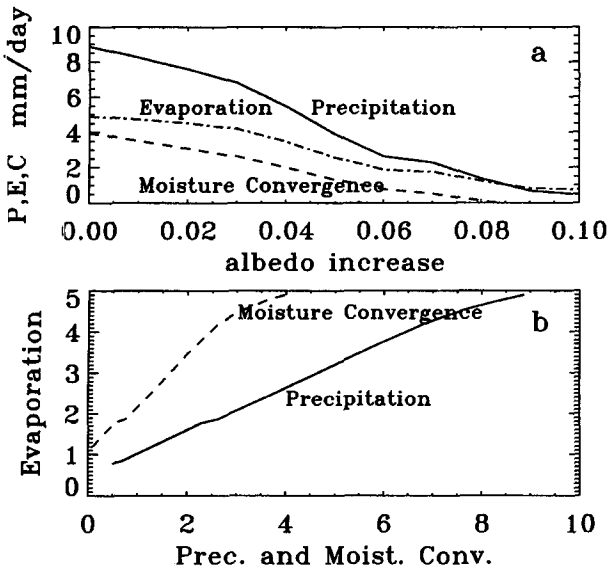


FIG. 14. Continuous deforestation: albedo increased. (a) Amazon average precipitation, evaporation, and moisture convergence change as albedo increases; (b) precipitation and moisture convergence plotted against evaporation. For January.

where $P$ is precipitation and $E$ is evaporation, and

$$\tilde{q} = q/q_0,$$

where $C_0 = \tilde{q}(1 - \tilde{q})^{-1}(\tilde{T}^* - \tilde{T})$ is the moisture convergence with vanishing evaporation; $C_0$ is about 1 mm day$^{-1}$ (Fig. 15) when albedo (therefore $T^*$) is fixed; and $q_0$ is the humidity at which latent heating of convergent moisture exactly balances adiabatic cooling. Here $q_0$ is independent of vertical velocity and determined by model parameters. The effect of moisture convergence is to reduce the atmospheric stability, and the model is unstable when humidity $q$ is greater than $q_0$ (cf. Davey and Gill 1987). The value of $q_0$ is found to be about 44 g kg$^{-1}$ in the current model. This is somewhat larger than for the Gill model because the vertical profile of latent heating puts less heat into the boundary layer.

The linear relation in Eq. (7) is obvious. When $E$ decreases from the control value to zero, $C$, $P$ decreases linearly to $C_0 = 1$ mm day$^{-1}$. Temperature $T$ changes slightly as a model response so that $C_0$ is not constant. In fact, $T$ varies almost linearly since the Eqs. (1) and (5) are quasi-linear within this range of evaporation change. However, the near straightness of the curve is still somewhat surprising for the slight nonlinearity and spatial averaging over model Amazon. In the case of albedo change, $C_0$ changes more but is still smaller than the other terms. At high albedo when sinking motion develops, $C_0$, which is proportional to IR heating, has become negative.

Using Eq. (7), given $C_0$, one can reproduce much of the numerical results in Fig. 14b and Fig. 15. For instance, for control run, $C_0 = 1$ mm day$^{-1}$, $E = 4.9$ mm day$^{-1}$, $q = 16$ g kg$^{-1}$, then

$$\tilde{q} = 16/44 = 0.36,$$

and using Eq. (7a) moisture convergence

$$C = 1 \text{ mm day}^{-1} + \frac{0.36}{1 - 0.36} 4.9 \text{ mm day}^{-1} = 3.8 \text{ mm day}^{-1},$$

which is quite close to the numerical value 4.0 mm day$^{-1}$ (Table 4).

Such relationships are simple and straightforward and can facilitate our understanding of the consequences of deforestation. In fact, the term $1 - \tilde{q}$ in Eq. (7) is similar to what is defined as "gross moist stability" by Neelin and Held (1987). Their reasonable success in modeling tropical low-level convergence based on a moist static energy budget supports our analysis. The oversimplification of the thermodynamic equation will be discussed in section 6.

Also plotted in Fig. 15 are Amazon deforestation results from some major GCM simulations. The control runs have large variations, so the precipitation and evaporation are scaled so that the control precipitations are all the same as that of the present model. With such scaling, three of the four GCM results are very close to each other. Without it, the differences between their control runs are often larger than the differences between control and deforestation runs. Even though the results in Lean and Rowntree (1993) are somewhat different from those in the other three studies, the slope

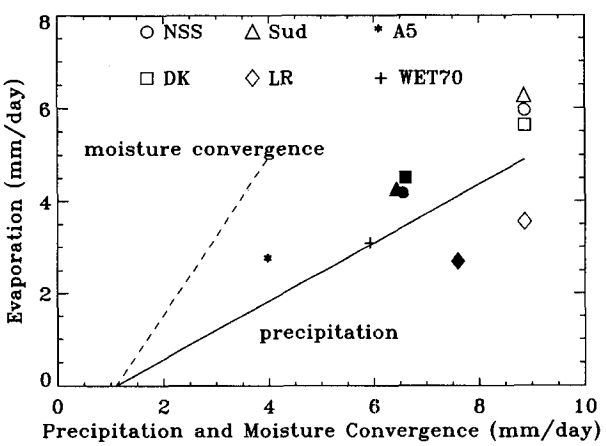


FIG. 15. Continuous deforestation: evaporation reduced. Also plotted are some GCM deforestation simulation results (precipitation versus evaporation) scaled by the control precipitation of present model. NSS is Nobre et al. (1991), DK is Dickinson and Kennedy (1992), LR is Lean and Rowntree (1993), Sud is Sud et al. (1995). A5 is experiment A5 of current model, WET70 is experiment WET70 of current model. Open symbols are for the control runs and filled symbols are for deforestation. Note that the model is for January and the GCMs are for annual average.

linking the open and filled symbols in Fig. 15 for each GCM study is similar among the four studies and is similar to that of our simple model. The implication is that Eq. (7) might be correct for our simple model and for various GCMs but that the coefficients in Eq. (7) might be different for different models due to their different numerical and physical formulations. In attempting to compare the GCM results to those of the model, one needs to be aware of some differences: the model is for January, whereas GCMs are for annual average, and the surface disturbances can be prescribed quite differently among the GCMs as well as the current model.

## 6. Summary and discussion

The impetus of this mechanistic model arises from our attempt to understand the consequences of Amazon deforestation. A reasonably good climatology is necessary to be able to draw credible conclusions from such an anomaly study. The model has to be self-consistent enough that it internally responds to land-surface change. Unlike much of the previous work with the Gill model, the present model contains essentially simplified primitive equations and predicts most of the major meteorological variables with few boundary conditions. In this sense, it is more like a GCM than like the Gill model.

Vertical structure is included in the model, although the resolution is not high. In addition to the baroclinic mode of the Gill model, it also contains the barotropic mode of motion and allows the specification of a vertical profile of convective latent heating. A GCM-like surface drag parameterization simulates the large damping necessary for obtaining realistic wind directions. Such a large damping has been hard to justify in the Gill model (Neelin 1988), so Li and Wang (1994) used diagnostic methods to obtain it.

In the parameterization of longwave radiation, a short (two day) Newtonian cooling time is used over the ocean, while it is 26 days over land. A short timescale over the ocean is hard to justify in terms of pure radiation consideration. However, the large heat capacity of the ocean maintains a "stagnant" SST. Through complex processes such as turbulent mixing and convection–radiation interaction, the SST plays a controlling role. A short relaxation time has to be used if Newtonian cooling parameterization is the choice. Model results indicate this is crucial in avoiding an overly wide ITCZ and the drifting of model-simulated lower atmosphere temperatures away from SST. Over land, control of surface temperature by solar insolation combined with albedo is physically based. It not only enables us to avoid too much convergence over the desert but also paves the way for the Amazon deforestation study.

Evaporation is parameterized by a bulk transfer formula. The surface wetness is proportional to precipitation. Both evaporation and moisture convergence are internally determined by the model. A direct water budget parameterization is used for convective precipitation, assuming a convectively unstable tropical atmosphere. Such convective instability of the tropical atmosphere has been questioned (e.g., Xu and Emanuel 1989), but, for a steady-state model, this is the most realistic parameterization available.

Overall, the model simulates well tropical climatology in light of its simplicity. The wind fields and convergence, and also precipitation and evaporation, are in reasonable agreement with observation. Fields that are generally not predicted by a simple model, such as temperature, wetness, and upper-level wind fields, bear at least a gross resemblance to the observations.

A number of weaknesses exist: unrealistically strong westerlies are simulated over major land masses in the summer hemisphere, perhaps a result of the neglect of nonlinear advection. The treatment of thermodynamics is less than satisfactory. Although the convective heating is generally much larger than IR heating, it acts primarily as a response to initial IR heating, resulting in a high sensitivity to SST over ocean and to solar insolation over land. Fu et al. (1994) showed that in a region between the Pacific ITCZ and SPCZ, the convection is largely suppressed due to a large-scale atmospheric sinking motion aloft, even though SST is high in this region. Conversely, regions with relatively low SST and strong convection are possible. Over land, factors such as topography and diurnal cycle play important roles in producing precipitation. The exclusion of such possibilities by the model originates from the fact that adiabatic cooling accompanying large-scale uplifting (therefore, convergence) is forced to immediately balance diabatic heating [Eq. (1e)]. In terms of model formulation, an important parameter $N$, the atmosphere buoyancy, is empirically derived from global average lapse rate. It is not totally clear what values this stability parameter should take in moist convective regions, and we see little justification for its use in the subtropical descending regions. Presumably the thermodynamic equation represents an interaction between the large-scale dynamics, radiation, and convection. This interaction is neither adequately understood nor well parameterized in GCMs. It requires a breakthrough in order to improve model thermodynamics in simple modeling. The inclusion of vertical structure takes one step toward such an improvement. We also anticipate that a time-dependent version of the present model would be necessary to allow a more realistic moisture budget and convective precipitation.

The climatic impact of Amazon deforestation has been explored in the context of this intermediate-level model. One important finding of the model is the high sensitivity of the tropical climate system to land-surface disturbance. This sensitivity results from the existence of a positive feedback loop in the South Amer-

ica–Atlantic atmospheric circulation system and hydrological cycle.

The high sensitivity of this loop is rooted in the fact that convective latent heating is the major driving force of the Walker–Hadley circulation, which, in turn, brings in the moisture needed for moist convection. The continent–ocean contrast is thought to be the ultimate cause of equatorial asymmetry (e.g., Stone and Chervin 1984). The land-surface disturbance of Amazon deforestation essentially reduces the "continentality" of the Amazon basin. This process is much like a warm episode of ENSO in the sense that a weaker Walker circulation accompanies a reduction in convective precipitation in the original rising branch. A similarly strong feedback exists except that the deforestation is a relatively permanent change in boundary conditions, while an El Niño event involves instability in the dynamics of the ocean–atmosphere interaction.

The model is sensitive to evaporation reduction because evaporation directly contributes to convective latent heating, in addition to moisture convergence feedback. The model is more sensitive to albedo change not only because of less infrared heating, but more importantly because the moisture convergence and evaporation both decrease drastically. Experiment A5_fixEq demonstrates that the system would be much less sensitive with evaporation and humidity held unchanged. Surface roughness length has an important effect by directly reducing evaporation. However, in the GCM simulation of Sud et al. (1995), the moisture convergence, not evaporation, is found to change substantially as surface roughness length changes. The pure dynamical effect of roughness length change shows an intriguing wind anomaly pattern but no significant change in the hydrology.

We explored the consequences of continuous deforestation. Results suggest that the climate system is largely able to sustain a dry surface at the location of the Amazon if a desert were placed there, but probably not a dry surface with low albedo. However, one needs to be cautious about these findings because such a large disturbance may move model simplifications outside their range of validity. The ocean may well have a significant response so as to alter the model results. Nonetheless, the model results point in an interesting direction and further study would be helpful in understanding paleoclimate in the Amazon and in other applications.

The weakening of the Hadley cell has further implications for teleconnection to midlatitude. Through weakening of the Walker circulation, Amazon deforestation can have some effect over central Africa.

The model also shows a decreased Atlantic SST gradient accompanying a weakened Walker–Hadley circulation. The degree of change depends on the coupling strength. With standard parameter values, a 1°C decrease in SST gradient across the equatorial Atlantic Ocean was found. Given the crudeness of both the atmospheric and ocean models, this probably only serves to raise the hypothesis. Our initial result also suggests the need for the GCM study to have an interactive ocean and to analyze its response and possible feedback. Through these analyses, we have quantified our hypothesis, as shown schematically in Fig. 2.

The roles of cloud feedback and solar absorption by atmosphere deserve some comments. Since shortwave absorption by atmosphere varies little with time, its change is negligible for the present model application purpose. The tuning parameter $\epsilon$ in Eq. (3d) can largely account for time-independent contributions from shortwave absorption by atmosphere and radiation effects of cloud. Clouds possess great variability, both spatially and temporally. The feedback of clouds to disturbances such as doubling of $CO_2$ has been simulated in a wide range by GCMs (Cess et al. 1989). ERBE observation (Ramanathan et al. 1989) shows a near cancellation of longwave and shortwave cloud forcing in the Tropics. This balance reflects the internal delicacy of deep convective clouds in the Tropics (Kiehl 1994). Therefore, one has reason to expect a similarly large cancellation between cloud longwave and shortwave radiative forcing anomalies if a disturbance such as Amazon deforestation is made such that total cloud cover decreases. This was found in Dickinson and Kennedy (1992), where a decrease in downward longwave radiation largely balanced the effect of penetrating solar radiation due to a reduction in cloud cover, leaving a net warming of the ground caused by the roughness length effect. However, the cancellation of cloud forcing at the top of the atmosphere does not necessarily imply the cancellation of all radiative effects. For instance, the extra solar radiation due to less cloud cover is mostly absorbed by the surface, while the longwave effect is directly felt by the whole atmospheric column as well as the surface. This can make a difference in the atmospheric stability. In fact, it is possible that this negative feedback could counteract the overly high sensitivity of the model to disturbance. Nevertheless, this competing effect of cloud radiative forcing largely negates the concerns about neglecting cloud feedback in the model.

Analysis of the model thermodynamic equation reveals that model response can be largely explained by thermodynamics alone within a predetermined convective region. The important implication here is that the existence of the strong positive feedback loop is rooted in model thermodynamics. The treatment of thermodynamics has a fundamental deficiency. Although the latent heating dominates in the diabatic heating term, the moisture convergence is largely determined by the initial infrared heating. Over land, although convection and precipitation roughly follow the seasonal variation of solar radiation, in reality, other factors may well initiate convection at favorable places where solar radiation is not so high. Once this happens, the latent heat released can be enough to sustain the convection. Such

a candidate to initiate convection is the diurnal cycle. During daytime, the surface temperature is high, the atmosphere can easily become unstable, and moist convection could occur provided that enough moisture is present. In this case, large-scale moisture convergence may not be necessary as a prerequisite for convection. An implication of this argument is that CISK-type parameterization would be insufficient in accounting for such a mechanism. On the other hand, places with high solar radiation may not be favored in terms of other conditions. Therefore, the present model probably overestimates the strength of the feedback loop and the sensitivity to land-surface disturbance. The extent of the overestimate is not clear at present. The only "evidence" is that none of the GCM experiments show a similarly large reduction in precipitation and evaporation (Fig. 15). We feel there is a strong need for both observation and modeling of tropical convective processes over land.

We conclude that the present model needs improvement for confident simulation of the climatic consequences of Amazon deforestation. While a number of improvements can be achieved relatively easily in some model parameterizations, the task to significantly improve the parameterization of the interaction among radiation, convection, and large-scale dynamics may not be straightforward and probably requires much better parameterization of cumulus convection and boundary-layer processes.

*Acknowledgments.* NZ thanks Drs. Robert Dickinson, Phil Krider, Bill Sellers, and Ben Herman for advising his Ph.D. dissertation, which includes the research reported here. We have benefited from discussions with Andrea Hahmann, James Shuttleworth, Carlos Nobre, David Neelin, Rong Fu, Richard Seager, E. Eltahir, and Fei-Fei Jin. We appreciate the insightful comments from the two anonymous reviewers and the editor, David A. Randall. Margaret Sanderson Rae is thanked for editing the final manuscript. This research was supported by NSF Grant ATM-9113163.

## APPENDIX

## Numerical Method

Equations (1a)–(1e), in combination with Eq. (5), are finite differenced on a staggered Arakawa C grid in the horizontal direction, while the vertical scheme is shown in Fig. 3, resulting in a matrix equation:

$$Ax = b,$$

where $x$ represents the five variables $U$, $V$, $\omega$, $\Phi$, and $T$ on each grid point in horizontal and vertical, and $A$ is a linear matrix, but $b = b(x)$ is a nonlinear function of $x$. Here $b$ includes nonlinear relationships in the thermodynamic equation, Eq. (5). Forcing is applied only within $\pm 30°$, and the surface drag can be a quadratic function of $U$. Sparse matrix technique is employed to decompose $A$ into two triangular matrices:

$$A = LU,$$

where $L$ is a lower triangular and $U$ is an upper triangular. Then iteration is used to solve the nonlinear matrix

$$x^{(n+1)} = A^{-1}b[x^{(n)}] = U^{-1}L^{-1}b[x^{(n)}],$$

where $n$ represents the $n$th iteration. Since LU decomposition is done only once, the back substitution needed for each iteration is highly efficient. The model was run on an IBM RISC/590. Without eliminating variables for the original five equations, the LU decomposition process took a few hours, while each iteration needed less than one second of CPU time. The iteration procedure converges quickly (Fig. 16). However, if the resolution goes higher, the computing time for the LU decomposition rises dramatically, approaching cubic dependence on resolution even though a sparse matrix technique is used (cf. Press et al. 1992). Eliminating four variables before finite differencing would allow compensation for a five-fold increase in resolution. The ocean model is solved in a similar fashion.

Zebiak (1986) has shown that the iteration procedure with convergence feedback numerically converges if the feedback term of the thermodynamic equation [the equivalent of Eq. (1e)] is smaller than the adiabatic cooling term. Otherwise the model numerically diverges and it represents a different climate regime (e.g., Gill 1982). We found this numerical convergence criterion holds for Eqs. (1a) and (1b), where $U$ or $V$ is the equivalent of $w$ in Eq. (1e). For instance, $\tau^x$ is proportional to $U$ in Eq. (1a). If we set $\alpha$ to be a

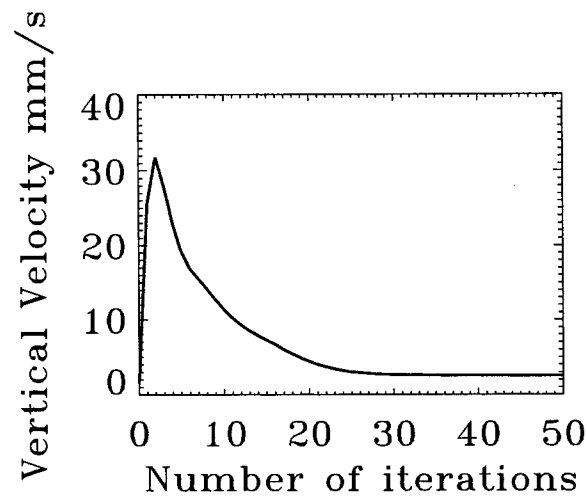


FIG. 16. Matrix solution convergence rate. Shown is the vertical velocity of a point in central Pacific ITCZ. Note: vertical velocity before iteration is that due to IR heating only and it approaches its final value (about twice the initial value at this location) at equilibrium. The large initial peak is related to surface drag.

large value in matrix decomposition, the addition of a term representing $\tau^x$ can be iterated until the model converges to the desired value. The advantage of doing so is that a variable on the right-hand side can be solved in a few seconds. This is especially useful if $\tau^x$ is parameterized as model dependent (even if it is a quadratic function of model wind). We did a standard von Neumann stability analysis for a simpler version of our model, which supports the numerical result, but analysis was not done for the full version including Eqs. (1) and (5) due to much algebraic complexity.

## REFERENCES


Arya, S. P., 1988: *Introduction to Micrometeorology.* Academic Press, 307 pp.

Betts, A. K., 1982: Saturation point analysis of moist convective overturning. *J. Atmos. Sci.*, **39,** 1484–1505.

Brubaker, K. L., D. Entekhabi, and P. S. Eagleson, 1993: Estimation of continental precipitation recycling. *J. Climate,* **6,** 1077–1089.

Cane, M. A., 1992: Tropical Pacific ENSO models: ENSO as a mode of the coupled system. *Climate System Modeling.* K. E. Trenberth, Ed., Cambridge University Press, 583–614.

Cess, R. D., and Coauthors, 1989: Interpretation of cloud-climate feedback as produced by 14 atmospheric general circulation models. *Science,* **245,** 513–516.

Charney, J. G., 1975: Dynamics of deserts and droughts in Sahel. *Quart. J. Roy. Meteor. Soc.,* **101,** 193–202.

——, and A. Eliassen, 1964: On the growth of the hurricane depression. *J. Atmos. Sci.,* **21,** 68–75.

Cornejo-Garrido, A. G., and P. H. Stone, 1977: On the heat balance of the Walker circulation. *J. Atmos. Sci.,* **34,** 1155–1162.

Cotton, W. R., and R. A. Anthes, 1989: *Storm and Cloud Dynamics.* Academic Press, 883 pp.

Davey, M. K., and A. E. Gill, 1987: Experiments on tropical circulation with a simple moist model. *Quart. J. Roy. Meteor. Soc.,* **113,** 1237–1269.

Deardorff, J. W., 1972: Parameterization of the planetary boundary layer for use in general circulation models. *Mon. Wea. Rev.,* **100,** 93–106.

DeMaria, M., 1985: Linear response of a stratified tropical atmosphere to convective forcing. *J. Atmos. Sci.,* **42,** 1944–1959.

Dickinson, R. E., 1992: Change in land use. *Climate System Modeling,* K. E. Trenberth, Ed., Cambridge University Press, 689–701.

——, and A. Henderson-Sellers, 1988: Modeling tropical deforestation: A study of GCM land-surface parameterizations. *Quart. J. Roy. Meteor. Soc.,* **114,** 439–462.

——, and P. J. Kennedy, 1992: Impacts on regional climate of Amazon deforestation. *J. Geophys. Res. Lett.,* **19,** 1947–1950.

——, A. Henderson-Sellers, and P. J. Kennedy, 1993: Biosphere-Atmosphere Transfer Scheme (BATS) Version 1e as coupled to the NCAR Community Climate Model. NCAR Tech. Note NCAR/TN-387+STR, 72 pp.

Dirmeyer, P. A., 1992: GCM studies of the influence of vegetation on the general circulation: The role of albedo in modulating climate change. Ph.D. thesis, University of Maryland, 227 pp.

Eltahir, E. A. B., and R. L. Bras, 1993: On the response of the tropical atmosphere to large-scale deforestation. *Quart. J. Roy. Meteor. Soc.,* **119,** 779–793.

——, and ——, 1994: Precipitation recycling in the Amazon basin. *Quart. J. Roy. Meteor. Soc.,* **120,** 861–880.

Emanuel, K. A., 1989: The finite amplitude nature of tropical cyclogenesis. *J. Atmos. Sci.,* **46,** 3431–3456.

Fu, R., A. D. Del Genio, and W. B. Rossow, 1994: Influence of ocean surface conditions on atmospheric vertical thermodynamic structure and deep convection. *J. Climate,* **7,** 1092–1108.

Gandu, A. W., and J. E. Geisler, 1991: A primitive equations model study of the effect of topography on the summer circulation over tropical South America. *J. Atmos. Sci.,* **48,** 1822–1836.

Geisler, J. E., 1981: A linear model of the Walker circulation. *J. Atmos. Sci.,* **38,** 1390–1400.

Gill, A. E., 1980: Some simple solutions for heat induced tropical circulation. *Quart. J. Roy. Meteor. Soc.,* **106,** 447–462.

——, 1982: Spontaneously growing hurricane-like disturbances in a simple baroclinic model with latent heat release. *Intense Atmospheric Vortices,* L. Bengtsson and M. J. Lighthill, Eds., Springer-Verlag, 111–129.

Hahmann, A. N., and R. E. Dickinson, 1995: Performance and sensitivity of the RCCM2/BATS model to tropical deforestation over the Amazon basin. *Conf. Proc. XXI IUGG General Assembly,* Boulder, CO.

Henderson-Sellers, A., and Gornitz, V., 1984: Possible climatic impacts of land cover transformations, with particular emphasis on tropical deforestation. *Clim. Change,* **6,** 231–157.

——, R. E. Dickinson, T. B. Durbidge, P. J. Kennedy, K. McGuffie, and A. J. Pitman, 1993: Tropical deforestation: Modeling local to regional scale climate change. *J. Geophys. Res.,* **98,** 7289–7315.

Hirst, A., 1986: Unstable and damped equatorial modes in simple coupled ocean–atmosphere models. *J. Atmos. Sci.,* **43,** 606–630.

Kiehl, J. T., 1994: On the observed near cancellation between longwave and shortwave cloud forcing in the tropical regions. *J. Climate,* **7,** 559–565.

Kleeman, R., 1989: A modeling study of the effect of the Andes on the summertime circulation of tropical South America. *J. Atmos. Sci.,* **46,** 3344–3362.

Lean, J., and Warrilow, D. A., 1989: Simulation of the regional climatic impact of Amazon deforestation. *Nature,* **342,** 411–413.

——, and Rowntree, P. R., 1993: A GCM simulation of the impact of Amazonian deforestation on climate using an improved canopy representation. *Quart. J. Roy. Meteor. Soc.,* **119,** 509–530.

——, C. B. Bunton, C. A. Nobre, and P. R. Rowntree, 1996: The simulated impact of Amazonian deforestation on climate using measured ABRACOS vegetation characteristics. *Quart. J. Roy. Meteor. Soc.,* in press.

Legates, D. R., and C. J. Wilmott, 1990a: Mean seasonal and spatial variability in gauge-corrected, global precipitation. *Int. J. Climatol.,* **10,** 111–128.

Li, T., and B. Wang, 1994: A thermodynamic equilibrium climate model for monthly mean surface winds and precipitation over the tropical Pacific. *J. Atmos. Sci.,* **51,** 1372–1385.

Lindzen, R. S., and S. Nigam, 1987: On the role of sea surface temperature gradients in forcing low-level winds and convergence in the Tropics. *J. Atmos. Sci.,* **45,** 2440–2458.

Matsuno, T., 1966: Quasi-geostrophic motions in equatorial areas. *J. Meteor. Soc. Japan,* **2,** 25–43.

McGuffie, K., A. Henderson-Sellers, H. Zhang, T. B. Durbidge, and A. J. Pitman, 1995: Global climate sensitivity to tropical deforestation. *Global Planet. Change,* in press.

Neelin, J. D., 1988: A simple model for surface stress and low-level flow in the tropical atmosphere driven by prescribed heating. *Quart. J. Roy. Meteor. Soc.,* **114,** 747–770.

——, and I. M. Held, 1987: Modeling tropical convergence based on the moist static energy budget. *Mon. Wea. Rev.,* **115,** 3–12.

Newell, R. E., J. W. Kidson, D. G. Vincent, and G. J. Boer, 1972: *The General Circulation of the Tropical Atmosphere.* Vol. 1, The MIT Press, 258 pp.

Nobre, C., P. J. Sellers, and J. Shukla, 1991: Amazonian deforestation and regional climate change. *J. Climate,* **4,** 957–988.

Philander, S. G. H., 1990: *El Niño, La Niña, and the Southern Oscillation.* Academic Press, 293 pp.

Polcher, J., and K. Laval, 1993: Statistical study of the regional impact of deforestation on climate using the LMD GCM. IAHS Publ. 214, 113–118.

Press, W. H., B. P. Flannery, S. A. Teukolsky, and W. T. Vetterling, 1992: *Numerical Recipes.* 2d ed., Cambridge University Press, 963 pp.

Priestly, C. H. B., and R. J. Taylor, 1972: On the assessment of surface heat flux and evaporation using large-scale parameters. *Mon. Wea. Rev.,* **100,** 81–92.

Ramanathan, V., B. R. Barkstrom, and E. F. Harrison, 1989: Climate and the earth's radiation budget. *Phys. Today,* **42,** 22–32.

Reynolds, R. W., 1988: A real-time global sea surface temperature analysis. *J. Climate,* **1,** 75–86.

Salati, E., 1987: The forest and the hydrological cycle. *The Geophysiology of Amazonia. Vegetation and Climate Interactions.* R. E. Dickinson, Ed., John Wiley and Sons, 273–296.

Seager, R., 1991: A simple model of the climatology and variability of the low-level wind field in the Tropics. *J. Climate,* **4,** 164–179.

Sellers, P. J., 1992: Biophysical models of land surface processes. *Climate System Modeling,* K. E. Trenberth, Ed., Cambridge University Press, 451–490.

Sellers, W. D., 1965: *Physical Climatology.* University of Chicago Press, 272 pp.

Shuttleworth, W. J., 1988: Evaporation from Amazonian rain forest. *Philos. Trans. Roy. Soc. London B,* **233,** 321–346.

Silva Dias, P. L., W. H. Schubert, and M. DeMaria, 1983: Large-scale response of the tropical atmosphere to transient convection. *J. Atmos. Sci.,* **40,** 2689–2707.

Stein, U., and P. Alpert, 1993: Factor separation in numerical simulations. *J. Atmos. Sci.,* **50,** 2107–2115.

Stone, P. H., and R. M. Chervin, 1984: The influence of ocean surface temperature gradient and continentality on the Walker circulation. Part II: Prescribed global changes. *Mon. Wea. Rev.,* **112,** 1524–1534.

Sud, Y. C., J. Shukla, and Y. Mintz, 1988: Influence of land surface roughness on atmospheric circulation and precipitation: A sensitivity study with a general circulation model. *J. Appl. Meteor.,* **27,** 1036–1054.

——, G. K. Walker, J.-H. Kim, G. E. Liston, P. J. Sellers, and W. K.-M. Lau, 1996: Biogeophysical consequences of a tropical deforestation scenario: A GCM simulation study. *J. Climate,* in press.

Wang, B., and T. Li, 1993: A simple tropical atmospheric model of relevance to short-term climate variation. *J. Atmos. Sci.,* **50,** 260–284.

Webster, P. J., 1972: Response of the tropical atmosphere to local steady forcing. *Mon. Wea. Rev.,* **100,** 518–541.

Williamson, D. L., J. T. Kiehl, V. Ramanathan, R. E. Dickinson, and J. J. Hack, 1987: Descriptions of NCAR Community Climate Model (CCM1), NCAR Tech. Note TN-285+STR, 112 pp.

Xu, K., and K. A. Emanuel, 1989: Is the tropical atmosphere conditionally unstable? *Mon. Wea. Rev.,* **117,** 1471–1479.

Zebiak, S. E., 1986: Atmospheric convergence feedback in a simple model for El Niño. *Mon. Wea. Rev.,* **114,** 1263–1271.

——, 1990: Diagnostic studies of Pacific surface winds. *J. Climate,* **3,** 1016–1031.

Zeng, N., 1994: Climatic impact of Amazon deforestation—explore underlying mechanism through simple modeling. Ph.D. thesis, University of Arizona, 114 pp.